Analysis of Bi and Trifilar Suspension Oscillations

Peter F. Hinrichsen
hinrichsen@videotron.ca

Contents

Symbol list

a	The vertical distance of the center of mass below the suspension points B-D.
$\bar{a}_{+,-}$	Acceleration vector.
a_r	Sway radial acceleration.
a_ϕ	Sway tangential acceleration.
A_0	Zero offset of Fourier component.
$A_{(2n-1)}$	Amplitude of the Fourier components.
b	Combined center of mass horizontal offset from the suspension symmetry axis.
c	Distance of the "body plus tray" CM from the symmetry axis of a trifilar suspension.
d, d_1, d_2	Half the spacing $2d$ of the parallel suspension lines.
d_1, d_2, d_3	The distances of the trifilar suspension lines from the center of mass.
$\bar{d}_i$	Vector positions of the ends of the suspension line.
$\bar{D}_{+,-}$	Drag force.
e	Extra displacement of CM from b to (b + e) from the symmetry axis
$E(k)$	The elliptical integral of the second kind.
$\bar{g}$	Acceleration due to gravity.
I	$I = \Sigma m_i r_i^2 = Mk^2$ Moment of Inertia about an axis through the CM.
k	Gyradius about an axis through the CM.
k	$k = Sin(\phi_0/2)$ for the elliptic integral transformation.
$K(k)$	Complete elliptical integral of the first kind.
k_{cm}	Gyradius about the combined CM of the body and tray plus added masses m
k_m	Yaw gyradius of the added mass m about the z axis through its CM.
k_{mo}	Yaw gyradius of the "body, tray and added mass m" about the symmetry axis.
k_o	Yaw gyradius of the "body" about the symmetry axis.
k_p	Pitch gyradius about the y axis through the CM.
k_T	Gyradius of the trifilar suspension tray.
k_y	Yaw gyradius of the suspended body.
k_{yT}	Gyradius of the offset body plus trifilar suspension tray.
k_{xx}	Gyradius about the principal x axis through the CM.
k_{yy}	Gyradius about the principal y axis through the CM.
k_{zz}	Gyradius about the principal z axis through the CM.
$\bar{l}_i$	Vectors representing the suspension lines.
L	The Lagrangian.
m	mass added for CM centering on a trifilar suspension.
m_i	Mass element at r_i from the rotation axis.
m_l	Mass of a suspension line $m_l = \lambda M$.
m_T	Mass of the trifilar suspension tray.
M	Mass of the suspended body, arithmetic-geometric mean.
M_T	Mass of the body plus trifilar suspension tray.
n	Number of oscillations per beat.
$N(x,1)$	Modified Arithmetic-Geometric Mean.

$\bar{P}$	Position vector of the point P.
q	The generalized co-ordinate for the Lagrangian.
r	Radius from the symmetry axis of the added masses m for CM centering.
$\bar{r}_i$	Vectors from the center of mass to the suspension points B and D.
r_i	Distance of a mass element from the rotation axis.
t_i	Zero crossing times.
t_0	Time offset.
$T, \vec{T}_1 \quad \vec{T}_2$	The tensions in the suspension lines 1 and 2.
T	Kinetic Energy.
T_l	Kinetic Energy of the suspension lines.
T_{beat}	The beat period between Yaw T_y and Sway T_s oscillations.
$T_{average}$	The average of the yaw period T_y and sway period T_s.
T_{so}	Zero amplitude sway oscillation period.
$T_s(\phi_0)$	Period of sway oscillation at amplitude ϕ_0.
T_{sm}	Zero amplitude Period of sway oscillation with finite mass suspension lines.
$T_y(\theta_o)$	Period of yaw rotational oscillation at amplitude θ_0.
T_{y1}	Yaw oscillation period with line spacing d_1.
T_{y2}	Yaw oscillation period with line spacing d_2.
T_{ye}	Yaw oscillation period with the CM displaced by an extra displacement e.
T_{yo}	Zero amplitude yaw oscillation period.
T_{ym}	Zero amplitude Period of yaw oscillation with finite mass suspension lines.
T_{yn}	Zero amplitude Period of yaw oscillation with added mass m.
T_{yT}	Yaw oscillation period of offset body plus trifilar tray.
U	Potential Energy.
U_l	Potential Energy of the suspension lines.
$\bar{V}$	Tangential velocity.
x	Out of plane horizontal displacement.
y	In plane horizontal displacement.
$\dot{y}$	In plane horizontal velocity.
$\ddot{y}$	In plane horizontal acceleration.
z	Vertical displacement of the ends of the suspension lines, i.e. of the hull CM.
$\dot{z}$	Vertical component of the velocity of the CM.
$\ddot{z}$	Vertical component of the acceleration of the CM.
$\ddot{z}_{Max}$	Maximum vertical component of the acceleration of the CM.
ε	Ratio $2d/l$ of the suspension spacing $2d$ to the suspension line length.
$\phi(t)$	The angles ϕ_1 and ϕ_2 that the suspension lines make with the vertical.
$\dot{\phi}$	Sway angular velocity.
$\ddot{\phi}$	Sway angular acceleration.
ϕ_0	Initial sway angular amplitude.
$\phi_{c1,2}$	Critical sway angles at which a line tension becomes zero.
ϕ_M	Sway angle at which the horizontal acceleration maximum occurs.

γ Ratio of added mass m to the body mass M.
η Angular displacements from θ_m for trifilar suspension CM centering.
η_m Angular displacements from θ_m for yaw period extremum for CM centering.
φ Angle of pitch about the body y axis, also integrand in the elliptic integral.
φ Angular position of second mass m on a trifilar suspension.
$\dot{\varphi}$ Pitch angular velocity.
$\ddot{\varphi}$ Pitch angular acceleration.
κ Ratio k_y/d of the yaw gyradius to half the line spacing.
λ Ratio m_l/M of the suspension line mass m_l to M that of the suspended body.
$v(\xi)$ Suspension line velocity at ξl from the upper suspension point.
θ Angular position of the compensation mass m on a trifilar suspension.
$\theta(t)$ The yaw angular displacement of the hull about a vertical axis.
$\dot{\theta}$ The yaw angular velocity about a vertical axis.
$\dot{\theta}_{Max}$ The maximum yaw angular velocity about a vertical axis.
$\ddot{\theta}$ The yaw angular acceleration about a vertical axis.
θ_m Yaw period extremum angle for mass m during trifilar suspension CM centering.
θ_0 Yaw angular amplitude.
θ_1, θ_2, θ_3 Angles between the vectors from the CM to the lines of a trifilar suspension
ρ Linear density of the suspension lines $\rho = m_l/l$.
$\bar{\Gamma}$ The torque due to the bifilar suspension.
ω Angular frequency of oscillation.
$\omega_{1,2}$ Double pendulum normal mode angular frequencies of oscillation.
ω_s Sway angular frequency of oscillation.
ξ Fractional distance down the suspension line length l to the point P.
ψ Roll angular displacement about the body x axis.
ψ Angular position of the body center of mass on a trifilar suspension.

Abstract

The theory of large angle oscillations both parallel and perpendicular to the plane and about the vertical symmetry axis of a bifilar suspension are presented and have been experimentally investigated using a smart phone. The horizontal, vertical and angular accelerations as well as the large amplitude periods of pendular and rotational oscillation were measured and compared with theory. The effect of finite mass suspension lines and of a center of mass displaced from the symmetry axis of the suspension are investigated. Simple period ratio measurements, which improve the precision of yaw and pitch gyradius measurement, are proposed. Many of the results also apply to trifilar suspensions.

I. Introduction

Estimation of the inertia properties of rigid bodies is important in the design of structures which rotate during their motion such as cars, boats, airplanes or satellites. In most cases accurate analytical models are not available and therefore the computational approaches cannot be used to estimate the inertia properties, and experimental measurements are required. The various methods of measuring the elements of the inertia tensor have been compared and evaluated by Schedlinski and Link[1], by Genta and Delprete[2], and a novel pendulum method is described by Bottasso et al[3].

For rotational motion the inertial properties of rigid bodies are specified by the moments of inertia about their principal axes and are $I = \Sigma m_i r_i^2 = Mk^2$ where the sum is over all mass elements m_i of the body and r_i are their perpendicular distances from the respective axes[4]. The moments of inertia therefore have dimensions of mass times a length squared and this “root mean square” length k is known as the gyradius or radius of gyration[5] about that axis. For any shaped body it is always possible to find a radius at which all the mass could be concentrated that would give the same moment of inertia, namely the gyradius, which can also be visualized as the half length of a symmetrical dumbbell of equal mass. The 3 x 3 inertia tensor can be graphically represented by an inertia ellipsoid of dimensions k_{xx}^{-1}, $k_{yy}^{-1}$and k_{zz}^{-1}along the three perpendicular principle axes[6]. The gyradius, which scales for bodies of the same shape, and is independent of the (uniform) density is a measure of the mass distribution and as such is used in the marine industry[7]. It is part of the rules for some Olympic sailboat classes[8] in order to control cost and insure that material is built into the ends to provide adequate structural integrity.

Although the physically relevant quantities are the elements of the inertia tensor, in a gravitational field the mass cancels and the equations are more simply expressed in terms of the gyradii, classic examples being the compound[9], double[10] and multi-filar pendula[11], as well as satellite dynamics. Although modern simulation programs calculate gyradii for every component, it is still often necessary to verify the results for complex structures experimentally[12], and such measurements serve to graphically illustrate the difference between the scalar mass and the tensor moment of inertia to students[4].

The bifilar suspension is known to almost all small children as a swing and although the pendular motion is the best known, for physicists it is the rotational oscillation about the symmetry axis that is commonly used to measure gyradii about a vertical axis[13,14,15,16]. However, the center of mass height and the gyradius about a

horizontal axis in the plane of the suspension can also be determined from the double pendulum oscillation perpendicular to the plane of the suspension[17]. Thus, even with the restriction to a parallel suspension, it is possible to measure all the elements of the inertia tensor of rigid objects, with reflection symmetry about their center planes, such as aeroplanes[18], UAVs[19,20,21] or boats[22,17].

A body on a bifilar suspension has four degrees of freedom and thus the general motion can be complex[16], however, by choosing the initial conditions appropriately the different modes of oscillation can be separately excited and for bodies suspended so as to rotate approximately about a principal axis the motion remains essentially only that mode. The present paper only treats the special cases of pure sway, pure yaw and double pendulum oscillations and assumes that coupling terms due to products of inertia are small. The Lagrangian theory of the motions can be simplified by appropriate choice of the four generalized coordinates appropriate to each of these motions. Furthermore the body center of mass (CM) is in the vertical plane of the suspension so its x location can be determined.

The trifilar suspension only has three degrees of freedom, i.e. no pitch or roll, and the sway and surge oscillations both have the simple pendulum period. The yaw results derived for the bifilar suspension can be directly applied to a trifilar suspension. However, the center of mass position is no longer determined and should be positioned on the symmetry axis of the suspension for the yaw oscillation not to be coupled to the sway-surge modes[23] although, as shown below, the error is generally small[24]. A five wire suspension[25] has only the yaw rotation degree of freedom and has achieved a precision of a part in 10^4 in moment of inertia[26] measurements.

The geometry of the suspension is determined by the length *l* of the suspension lines and their spacing *2d*, or the non-dimensional ratio $\varepsilon = 2d/l$. In general $\varepsilon < 1$ and for $\varepsilon > 1$ the maximum angle of yaw is $\theta_0 = \text{Asin}\varepsilon^{-1}$. The dynamics are determined by the elements of the inertia tensor of the suspended body, as, in the absence of damping, the mass cancels. Thus the yaw rotation can be characterized by the yaw gyradius k_y, or the non-dimensional ratio $\kappa = k_y/d$. Then if times are expressed in terms of t/T_{so}, where $T_{so} = 2\pi\sqrt{(l/g)}$ is the small angle sway period, the equations of motion can be expressed in non-dimensional form.

A number of variations of the bifilar suspension have been described by Cromer[14] so this paper will restrict itself to the symmetrical equal length parallel line suspension, from two points at the same level. Such bifilar suspensions have been used by the author to measure the yaw gyradii of sailboats competing in the Olympic games, and to compare the yaw gyradius with the pitch gyradius as measured with the standard compound pendulum technique[17,22,27]. Hence the use of nautical terms to describe the various motions.

The measurement of the period of angular oscillation for determining yaw gyradii is well known and has been used in the 1920s for measurements of full size aircraft[18] and more recently for UAVs[19,20,21]. A significant problem in such zero crossing timing data is the modulation of the measured yaw period by lateral sway motion in the plane of the suspension, which must therefore be eliminated by using precise initial conditions. This, however, can be turned to advantage by using the beat frequency between these

motions, or a FFT[28], to derive the yaw gyradius, thus eliminating a number of the variables.

For sway oscillation in the plane of a symmetrical parallel suspension the body does not rotate so this is the motion of a simple pendulum and an accelerometer, such as that in the iPhone 4 or available from Gulf Coast[29], will measure the horizontal and vertical accelerations, which for large amplitudes deviate significantly from being sinusoidal.

The MEMS gyro-accelerometer in the iPhone[30], or that in a Micro Strain[31] were used to study the rotational oscillations of the suspension and have the advantage of providing simultaneous three axis rotational velocities and linear accelerations, so that extraneous motions can be monitored, as well as allowing the detailed study of motions involving more than one degree of freedom. This separation of the sway and yaw oscillation data allows simple and precise yaw gyradius measurements from simultaneous or consecutive excitation of these motions. In practice it is difficult to excite one of these two oscillations without some of the other, and the sensitivity of the instrument is such that it records them both.

All the measurements described in this paper can be inexpensively made with a smart phone (many of which are being discarded so are available free!), NODE+[32] (or other MEMS gyros) and some string, and can easily be extended to real life objects of interest to students, such as model boats, aircraft, drones, cars, footballs, golf clubs, tennis racquets and baseball bats to mention just a few. In these days of budgetary constraints on laboratory equipment this is a significant advantage. However, the sophistication of the analysis of the results can be tailored the level of a variety of classical mechanics courses.

II. Sway Theory

A. 2D in plane Sway Oscillation Accelerations

The lateral oscillation of an equal length parallel bifilar pendulum in the y-z plane of the suspension does not involve any rotation of the suspended object, so is described in terms of the generalized coordinates $\phi = \phi_1 = \phi_2$, the angle the suspension lines make with the vertical, and the roll, pitch and yaw angles $\varphi = \psi = \theta = 0$. For suspension lines of negligible mass and in the absence of dissipative forces, the small angle period is that of a simple pendulum[33,34,35,9]

$$T_{s0} = 2\pi\sqrt{\frac{l}{g}} \tag{0.1}$$

Note that "*l*" is the length from the pivot points A and C at the fixed support to the suspension points B and D, see figure 1, and is independent of the position of the center of mass of the suspended object, which therefore does not have to be known. This has the advantage that changes due to mounting the MEMs gyro or bearings etc. do not affect the period $T_s(\phi)$. For in plane oscillation of a parallel bifilar suspension the two tensions in the support lines are parallel and can be combined into a single force $T = T_1 + T_2$, see figure 2. The resulting acceleration for a simple pendulum have been discussed by a number of authors [36, 37,38,39,40,41].

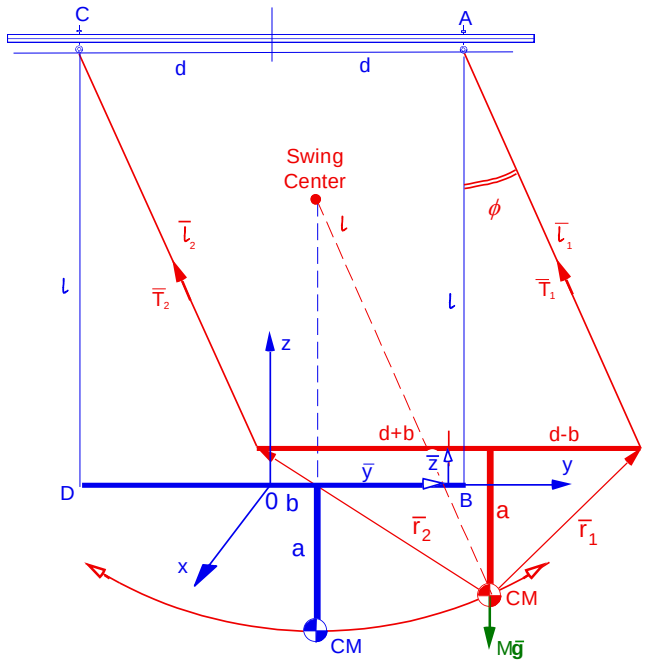

Figure 1 *Sway oscillation in the y-z plane of a parallel bifilar suspension with spacing 2d and length l, of a body of mass M with its center of mass a distance "a" below the center of the suspension and offset by a distance "b".*

For no damping and release from rest at an initial angular displacement ϕ_0 the velocity at displacement ϕ, as derived from energy conservation, is given by

$$\frac{1}{2}Ml^2\dot{\phi}^2 = Mgl\left(Cos\phi - Cos\phi_0\right) \tag{0.2}$$

The radial and tangential accelerations are

$$a_r = l\dot{\phi}^2 = 2g\left(Cos\phi - Cos\phi_0\right) \qquad a_\phi = -gSin\phi \tag{0.3}$$

So the vertical and horizontal components of the acceleration are

$$\begin{aligned} \ddot{y} &= -g(3Cos\phi - 2Cos\phi_0)Sin\phi \\ \ddot{z} &= g\left\{(3Cos\phi - 2Cos\phi_0)Cos\phi - 1\right\} \end{aligned} \tag{0.4}$$

$$\ddot{y}(0) = 0 \qquad \ddot{y}(\phi_0) = -gSin\phi_0 Cos\phi_0$$
$$\ddot{z}(0) = 2g(1 - Cos\phi_0) \qquad \ddot{z}(\phi_0) = -gSin^2\phi_0$$

From which, in the absence of damping, the angular displacement, velocity and amplitude can, without the approximation of small angle sinusoidal motion, be derived as:

$$Tan\phi = \frac{-\ddot{y}}{\ddot{z} + g} \tag{0.5}$$

$$Cos\phi_0 = \frac{\ddot{y}/g + 3Cos\phi Sin\phi}{2Sin\phi} = \frac{3Cos^2\phi - 1 - \ddot{z}/g}{2Cos\phi} = \frac{\left(2g - \ddot{z}\right)\left(\ddot{z} + g\right) - \ddot{y}^2}{2g\sqrt{\ddot{y}^2 + \left(\ddot{z} + g\right)^2}} \tag{0.6}$$

$$\dot{\phi}^2 = \frac{\ddot{y}^2 + \ddot{z}\left(\ddot{z} + g\right)}{l\sqrt{\ddot{y}^2 + \left(\ddot{z} + g\right)^2}} \tag{0.7}$$

It is interesting to note that the acceleration does not depend on the length of the suspension, and hence on its period, but depends only on the initial angle ϕ_0 and the angular position ϕ. Thus each half cycle of the oscillation is the same, except that the sign of $\ddot{y}$ changes, so the horizontal component has the period of the pendulum while the vertical component has half that period and exceeds "*g*" at $\phi = 0$ for $\phi_0 > 60$ degrees.

For large amplitudes the variation of $\ddot{y}$ and $\ddot{z}$ with time become significantly non sinusoidal. As the angle ϕ decreases from ϕ_0, the velocity and hence the radial acceleration and tensions, increase leading to an increase in the horizontal component of the acceleration which, however, for low amplitudes ϕ_0 this is dominated by the Sinϕ term. For larger amplitudes the former initially dominates the Sinϕ term, leading to maxima in the horizontal acceleration, before it decreases to zero at the equilibrium position.

For $\phi_0 > \pi/6$ the horizontal acceleration $\ddot{y}(\phi_0)$ becomes a local minimum and as expected is zero for $\phi_0 = \pi/2$. Then the angle at which the maxima occur are given by

$$\frac{d\ddot{y}}{d\phi} = 6Cos^2\phi_M - 2Cos\phi_0 Cos\phi_M - 3 = 0 \tag{0.8}$$

From which one can see that for $\phi_0 < \pi/6$ (30^0) $\phi_M > \phi_0$ so ϕ_M is not physical[39].

For $\phi_0 > \pi/6$ $\phi_M < \phi_0$ and

$$Cos\phi_M = \frac{Cos\phi_0 + \sqrt{Cos^2\phi_0 + 18}}{6} \tag{0.9}$$

Then expanding the time variation of the angular displacement as a Fourier series $\phi(t) = \Sigma\, \phi_i\, Sin(2n_i\text{-}1)\omega_0 t$, with $\omega_0 = \sqrt{g/l}$, and for amplitudes $\phi_0 < 1$ keeping only the first term:

$$\begin{aligned} a_r &= g\phi_0^2 Sin^2\omega_0 t \qquad a_\phi = -g\phi_0 Cos\omega_0 t \\ \ddot{y} &\approx -g\phi_0 \left\{\phi_0 Sin^2\omega_0 t\ Sin\left(\phi_0 Cos\omega_0 t\right) + Cos\omega_0 t\ Cos\left(\phi_0 Cos\omega_0 t\right)\right\} \\ \ddot{z} &\approx g\phi_0 \left\{\phi_0 Sin^2\omega_0 t\ Cos\left(\phi_0 Cos\omega_0 t\right) - Cos\omega_0 t\ Sin\left(\phi_0 Cos\omega_0 t\right)\right\} \end{aligned} \tag{0.10}$$

B. Sway Oscillation Suspension Line Tensions

For pure sway motion of a parallel bifilar suspension the suspended body does not rotate about its center of mass and therefore the net torque on the suspended body must be zero. Thus if the center of mass is at the center of the line B-D the tensions T_1 and T_2 are equal, which however this is not in general the case. The situation when the center of mass is offset by "*b*" from the center of the suspension and a distance "*a*" below it, is shown in figure 1.

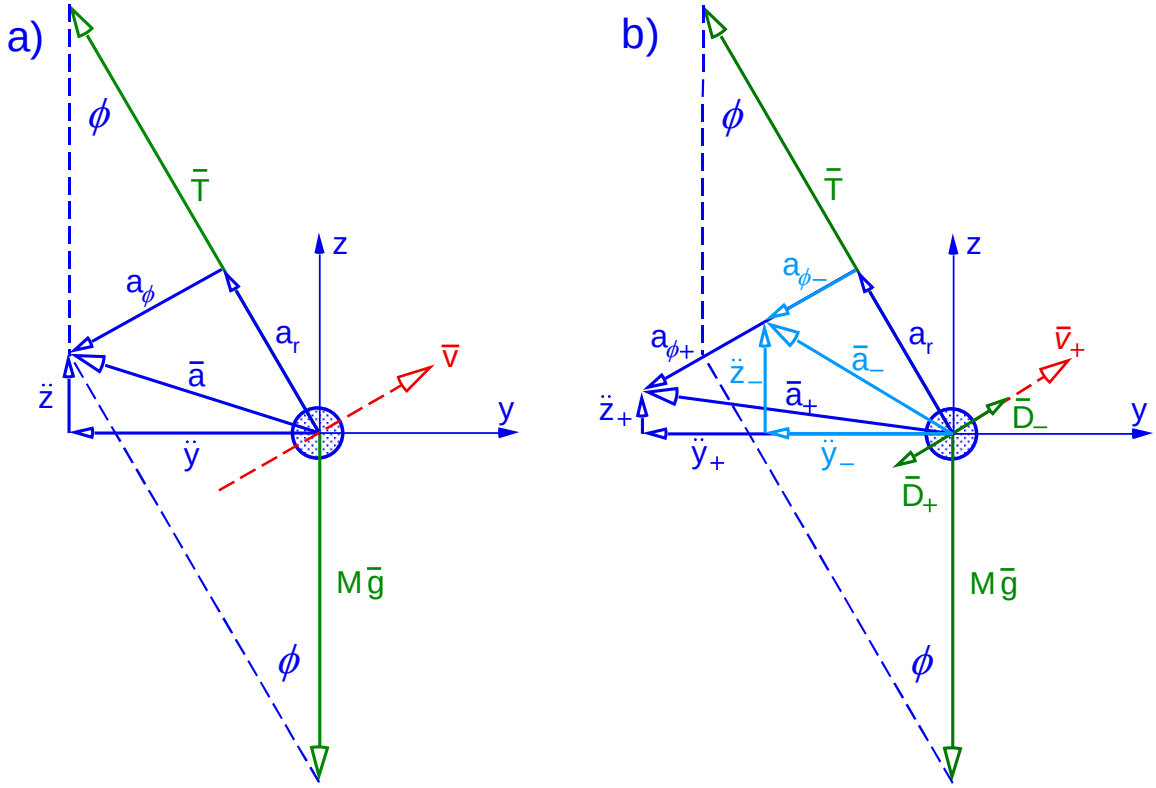

Figure 2 *Vector diagram, a) in the absence of damping and b) with damping **D** (for positive and negative velocity), showing the weight M**g** and the sum of the tensions **T** = **T₁**+**T₂** acting on the suspended body. The body has velocity **V**, and the resultant acceleration **a** is resolved into either the radial a_r and tangential a_ϕ, or the vertical $\ddot{z}$ and horizontal $\ddot{y}$ components.*

Resolving the forces in the direction of the suspension lines, as shown in figure 2, with **T** = **T₁**+**T₂**

$$T - MgCos\phi = Ma_r = Ml\dot{\phi}^2 = 2Mg(Cos\phi - Cos\phi_0) \tag{0.11}$$

So

$$T = T_1 + T_2 = Mg(3Cos\phi - 2Cos\phi_0) \tag{0.12}$$

The net torque about the center of mass is:

$$\vec{\Gamma} = \mathrm{T}_1\left\{-a\,y/l-\left(d-b\right)\left(1-z/l\right)\right\}+\mathrm{T}_2\left\{-a\,y/l+\left(d+b\right)\left(1-z/l\right)\right\}=0 \qquad (0.13)$$

Then substituting for $y = l\,\mathrm{Sin}\phi$, $z = l\,(1-\mathrm{Cos}\phi)$ and equating

$$\vec{T}_1 = \frac{Mg}{2}(3Cos\phi - 2Cos\phi_0)\left\{1+\frac{b-aTan\phi}{d}\right\}\begin{pmatrix}0\\ Sin\phi\\ Cos\phi\end{pmatrix}$$
$$\vec{T}_2 = \frac{Mg}{2}(3Cos\phi - 2Cos\phi_0)\left\{1+\frac{aTan\phi-b}{d}\right\}\begin{pmatrix}0\\ Sin\phi\\ Cos\phi\end{pmatrix} \qquad (0.14)$$

The parameter "*b*" can be deduced from static measurements, but also from a fit of equations(0.14) to the dynamic data. Note that T_1 goes negative for angles ϕ greater than critical angles $\phi_{c1} = Atan[(d+b)/a]$ and T_2 for $\phi_{c2} = Atan[-(d-b)/a]$, i.e. one suspension line goes slack and the above equations no longer apply, or if suspension rods are used one is in compression. For lines and angles larger than ϕ_c the motion becomes that of a double pendulum with $l_1 = l_i$ and $l_2 = r_i$ until the second suspension line again becomes taught.

C. Sway Oscillation period, massless lines

For the sway oscillation the angular velocity of the suspension lines is given by equation(0.2) as:

$$\dot{\phi} = \pm\sqrt{\frac{2g}{l}\left(Cos\phi_0 - Cos\phi\right)} = \pm\frac{4\pi}{T_{s0}}\sqrt{\left[Sin^2\left(\phi_0/2\right) - Sin^2\left(\phi/2\right)\right]} \tag{0.15}$$

Then with the substitutions $Sin\left(\phi/2\right) = Sin\left(\phi_0/2\right)Sin\varphi$ and $k = Sin\left(\phi_0/2\right)$. The inverse can be integrated to give the period of oscillation as[9,35]

$$\begin{aligned} T_s\left(\phi_0\right) &= 2\sqrt{\frac{l}{g}}\int_0^{\theta_0}\frac{1}{\sqrt{Sin^2\left(\phi_0/2\right) - Sin^2\left(\phi/2\right)}}d\phi = 4\sqrt{\frac{l}{g}}\int_0^{\pi/2}\frac{d\varphi}{\sqrt{1-k^2Sin^2\varphi}} \\ &= 4\sqrt{\frac{l}{g}}K\left(k\right) = \frac{2\pi}{M\left(\sqrt{1-k^2},1\right)}\sqrt{\frac{l}{g}} = \frac{T_{s0}}{M\left(Cos\left(\theta_0/2\right),1\right)} \end{aligned} \tag{0.16}$$

Where $T_{s0} = 2\pi\sqrt{l/g}$ is the zero amplitude period, *K(k)* is the complete elliptical integral of the first kind[42] and is often evaluated as a series expansion[9,35]

$$T_s\left(\phi_0\right) = T_{s0}\left\{1 + \frac{1}{16}\phi_0^2 + \frac{11}{3072}\phi_0^4 + \frac{173}{737280}\phi_0^6 \ldots\right\} \tag{0.17}$$

A number of other approximate series expansions have been proposed [14,35,9,43,44,45], however, *K(k)* can be simply calculated from the arithmetic-geometric mean[42,46,47] $M\left(Cos\left(\theta_0/2\right),1\right) = \pi/\left\{2K\left(k\right)\right\}$ which rapidly converges to a precise value, and is especially useful for large angular amplitudes.

D. Sway Oscillation period with finite mass lines

For a bifilar suspension with linear parallel suspension lines, each of mass $m_l = \lambda M$, the potential and kinetic energies are:

$$T = \left(Ml^2/2\right)\dot{\phi}^2 + \left(m_l l^2/3\right)\dot{\phi}^2 = \left(Ml^2/2\right)\{1+2\lambda/3\}\dot{\phi}^2 \tag{0.18}$$

$$U = Mgl\left(1-\mathrm{Cos}\,\phi\right) + m_l gl\left(1-\mathrm{Cos}\,\phi\right) = Mgl\left(1+\lambda\right)\left(1-\mathrm{Cos}\,\phi\right) \tag{0.19}$$

which when included in the Lagrangian[6] lead to:

$$\begin{aligned} Ml^2\{1+2\lambda/3\}\ddot{\phi} &= -Mgl\left(1+\lambda\right)\mathrm{Sin}\,\phi \\ \ddot{\phi} &\approx -\frac{g\left(1+\lambda\right)}{l\{1+2\lambda/3\}}\phi \end{aligned} \tag{0.20}$$

So the small angle sway period with massive suspension lines T_{sm} is[48,49,50]:

$$T_{sm} = 2\pi\sqrt{\frac{l}{g}}\sqrt{\frac{\left(1+2\lambda/3\right)}{\left(1+\lambda\right)}} \approx T_{so}\left(1-\frac{\lambda}{6}\right) + O\left(\lambda^2\right) \tag{0.21}$$

E. Sway Fourier Components

The amplitudes of the Fourier components of the large angle oscillation of a simple pendulum were numerically evaluated by Simon & Reisz[51] and a perturbation expansion of the solution to the pendulum equation is given by Fulcher & Davis[52],[53] was modified by Belendez[54], and fits the numerical calculation[51] for angles less than 2 radians. Riccardo Borghi[55] and Salvador Gil et.[56] A. further investigated the Fourier approach to the pendulum.

$$\begin{aligned}\phi(t) = &\left\{\phi_0 + \phi_0^3/192 + 17\phi_0^5/61440\right\} Cos(\omega t) \\ &- \left\{\phi_0^3/192 + \phi_0^5/3072\right\} Cos(3\omega t) + \left\{\phi_0^5/20480\right\} Cos(5\omega t) + ...\end{aligned} \tag{0.22}$$

The large amplitude bifilar yaw oscillation deviates from sinusoidal in a similar manner, but the detailed behaviour depends on both ε^2 and κ^2.

III. Yaw Rotation Theory

F. Yaw Oscillation Lagrangian, centered with massless lines

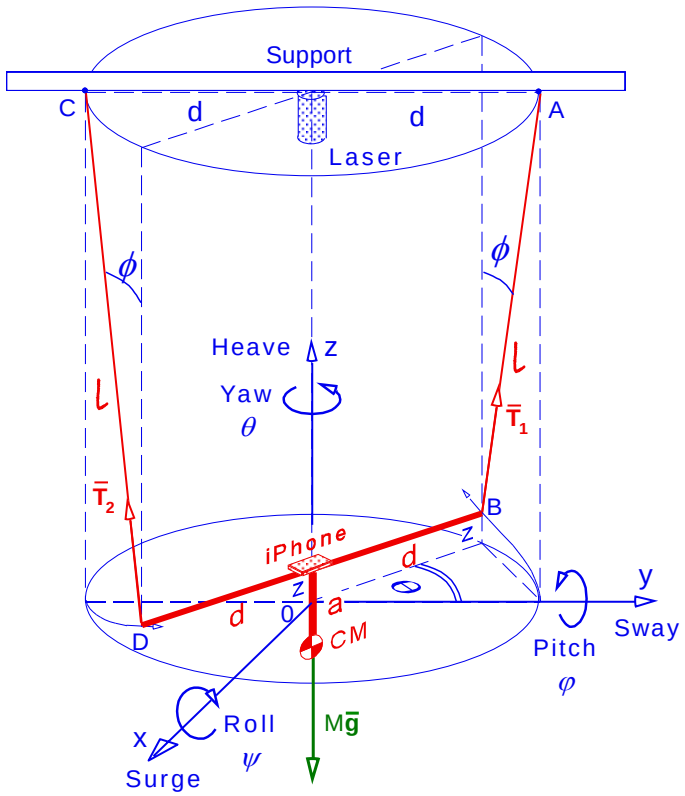

Figure 3 *Rotation about the vertical symmetry axis of a parallel bifilar suspension, with spacing 2d and length l, of a body of mass M with its center of mass a distance "a" below the center of the suspension points B-D.*

For a rotational displacement θ about the vertical symmetry axis of a suspension of length *l* and spacing 2*d* the torque due to the tension in the suspension lines is $\Gamma = 2Td\ Sin\phi\ Cos(\theta/2) = Td\varepsilon Sin\theta = Mk_y^2\ddot{\theta}$ and the tensions are

$$T = M(\ddot{z}+g)/2Cos\phi = M(\ddot{z}+g)/2\sqrt{1-\varepsilon^2 Sin^2(\theta/2)} \tag{0.23}$$

So

$$\ddot{\theta} = \frac{(\ddot{z}+g)}{\kappa^2 l\sqrt{1-\varepsilon^2 Sin^2(\theta/2)}}Sin\theta \tag{0.24}$$

Where $\varepsilon = 2d/l$ and $\kappa = k_y/d$. For small angular displacement the tension can be approximated as $T \approx Mg/2$ leading to a differential equation with an oscillatory solution of period $T_{y0} = \left(2\pi k_y/d\right)\sqrt{l/g}$ [15]. However for larger angular displacement the vertical acceleration has to be included.

For a body of mass *M*, with its center of mass on the vertical symmetry axis of an equal length parallel bifilar suspension of negligible mass and torsional rigidity, see figure 3, the vertical displacement from the equilibrium position, when it is rotated by an angle θ about the vertical symmetry axis is:

$$z = l - \sqrt{l^2 - 2d^2\left(1 - Cos\theta\right)} = l\left\{1 - \sqrt{1 - \varepsilon^2 Sin^2\left(\theta/2\right)}\right\} \approx \left(\frac{d^2}{2l}\right)\theta^2 + \ldots \tag{0.25}$$

Where *l* is the length, 2*d* the spacing and $\varepsilon = 2d/l$ for the suspension.

Then in terms of the angular motion the vertical velocity and acceleration are:

$$\left|\dot{z}\right| = \frac{d^2 Sin\theta}{\sqrt{l^2 - 2d^2\left(1 - Cos\theta\right)}}\dot{\theta} = \left(\frac{d^2}{l}\right)\frac{Sin\theta}{\sqrt{1 - \varepsilon^2 Sin^2\left(\theta/2\right)}}\dot{\theta} \tag{0.26}$$

$$\left|\ddot{z}\right| = \left(\frac{d^2}{l}\right)\left[\frac{Sin\theta}{\sqrt{1 - \varepsilon^2 Sin^2\left(\theta/2\right)}}\ddot{\theta} + \frac{\left\{Cos\theta + \varepsilon^2 Sin^4\left(\theta/2\right)\right\}}{\left\{1 - \varepsilon^2 Sin^2\left(\theta/2\right)\right\}^{3/2}}\dot{\theta}^2\right] \tag{0.27}$$

So the potential energy *U* and kinetic energy *T* are:

$$U = Mgz = Mgl\left(1 - \sqrt{1 - 2(d/l)^2(1 - Cos\ \theta)}\right) = Mgl\left(1 - \sqrt{1 - \varepsilon^2 Sin^2\left(\theta/2\right)}\right) \tag{0.28}$$

and

$$\begin{aligned} T &= \frac{1}{2}Mk_y^2\dot{\theta}^2 + \frac{1}{2}M\dot{z}^2 = \frac{1}{2}Mk_y^2\left\{1 + \frac{\varepsilon^2 Sin^2\left(\theta/2\right)Cos^2\left(\theta/2\right)}{\kappa^2\left[1 - \varepsilon^2 Sin^2\left(\theta/2\right)\right]}\right\}\dot{\theta}^2 \\ \text{or} \qquad &= \frac{1}{2}M\left\{1 + \frac{\kappa^2\left[1 - \varepsilon^2 Sin^2\left(\theta/2\right)\right]}{\varepsilon^2 Sin^2\left(\theta/2\right)Cos^2\left(\theta/2\right)}\right\}\dot{z}^2 \end{aligned} \tag{0.29}$$

Where $\kappa = k_y/d$, with k_y the yaw gyradius of the suspended body about a vertical axis through its center of mass.

For release from rest at an initial yaw angle θ_0, and in the absence of dissipative forces, conservation of energy leads to:

$$\frac{1}{2}Mk_y^2\left\{1+\frac{\varepsilon^2 Sin^2\left(\theta/2\right)Cos^2\left(\theta/2\right)}{\kappa^2\left[1-\varepsilon^2 Sin^2\left(\theta/2\right)\right]}\right\}\dot{\theta}^2 = Mgl\left(\sqrt{1-\varepsilon^2 Sin^2\left(\theta/2\right)}-\sqrt{1-\varepsilon^2 Sin^2\left(\theta_0/2\right)}\right) \quad (0.30)$$

So the angular velocity is:

$$\dot{\theta}^2 = \left(\frac{g}{l}\right)\frac{8\left[1-\varepsilon^2 Sin^2\left(\theta/2\right)\right]\left(\sqrt{1-\varepsilon^2 Sin^2\left(\theta/2\right)}-\sqrt{1-\varepsilon^2 Sin^2\left(\theta_0/2\right)}\right)}{\varepsilon^2\left\{\kappa^2-\varepsilon^2 Sin^2\left(\theta/2\right)\left(\kappa^2-Cos^2\left(\theta/2\right)\right)\right\}} \quad (0.31)$$

The maximum value occurs at the equilibrium position and is

$$\dot{\theta}_{Max}^2 = \frac{8g\left(1-\sqrt{1-\varepsilon^2 Sin^2\left(\theta_0/2\right)}\right)}{\varepsilon^2\kappa^2 l} \approx \frac{g\theta_0^2}{l\kappa^2}+\ldots \quad (0.32)$$

Now substituting equation(0.31) into equation(0.26) gives $\dot{z}^2$ in terms of the angular motion

$$\dot{z}^2 = \left(\frac{gl}{2}\right)\frac{\varepsilon^2\left(\sqrt{1-\varepsilon^2\,\mathrm{Sin}^2\left(\theta/2\right)}-\sqrt{1-\varepsilon^2\,\mathrm{Sin}^2\left(\theta_0/2\right)}\right)}{\left[\kappa^2-\varepsilon^2 Sin^2\left(\theta/2\right)\left(\kappa^2-Cos^2\left(\theta/2\right)\right)\right]}Sin^2\theta \quad (0.33)$$

Substituting θ_0 from equation(0.31) into its time derivative, or alternatively via the Lagrangian, leads to the nonlinear differential equation:

$$\left(\kappa^2+\frac{\varepsilon^2 Sin^2\theta}{4\left\{1-\varepsilon^2 Sin^2\left(\theta/2\right)\right\}}\right)\ddot{\theta}+\frac{\varepsilon^2\left\{Cos\theta+\varepsilon^2 Sin^4\left(\theta/2\right)\right\}Sin\theta}{4\left\{1-\varepsilon^2 Sin^2\left(\theta/2\right)\right\}^2}\dot{\theta}^2+\frac{g}{l\sqrt{1-\varepsilon^2 Sin^2\left(\theta/2\right)}}Sin\theta=0 \quad (0.34)$$

Or in terms of the angular motion for amplitude θ_0

$$\ddot{\theta}=\frac{-g\sqrt{1-\varepsilon^2 Sin^2\left(\theta/2\right)}}{\kappa^2 l\left\{1-\varepsilon^2 Sin^2\left(\theta/2\right)\left(1-\kappa^{-2}Cos^2\left(\theta/2\right)\right)\right\}}\left\{1+\frac{2\left\{Cos\theta+\varepsilon^2 Sin^4\left(\theta/2\right)\right\}\left(\sqrt{1-\varepsilon^2 Sin^2\left(\theta/2\right)}-\sqrt{1-\varepsilon^2 Sin^2\left(\theta_0/2\right)}\right)}{\left\{\kappa^2-\varepsilon^2 Sin^2\left(\theta/2\right)\left(\kappa^2-Cos^2\left(\theta/2\right)\right)\right\}\sqrt{1-\varepsilon^2 Sin^2\left(\theta/2\right)}}\right\}Sin\theta \quad (0.35)$$

For the special case of $\varepsilon = 1$ this simplifies to

$$\left(\kappa^2+Sin^2\left(\theta/2\right)\right)\ddot{\theta}+\frac{Sin\theta}{4}\dot{\theta}^2+\left(\frac{g}{l}\right)2Sin\left(\theta/2\right)=0 \quad (0.36)$$

For small angles θ it reduces to:

$$\left\{1+\left(\frac{\varepsilon}{2\kappa}\right)^2\theta^2\right\}\ddot{\theta}-\left(\frac{\varepsilon}{2\kappa}\right)^2\theta\dot{\theta}^2\approx-\frac{g}{\kappa^2 l}\theta \tag{0.37}$$

A trial solution[57] of the form $\theta(t)=\theta_0 Cos\left(2\pi t/T_y\right)$ then leads to a solution with yaw period:

$$T_y\left(\theta_0\right)\approx 2\pi\kappa\sqrt{\frac{l}{g}}\left\{1+\frac{\theta_0^2}{16}\left(1-\frac{3\varepsilon^2}{4}+\frac{\varepsilon^2}{\kappa^2}\right)\right\} \tag{0.38}$$

So the zero amplitude the yaw period[15,14] is $T_{y0}=2\pi k_y/d\sqrt{l/g}$ and is the basis of the bifilar suspension method of measuring moments of inertia $I_y=Mk_y^2$ as:

$$k_y=\frac{T_{y0}d}{2\pi}\sqrt{\frac{g}{l}}=\frac{T_{y0}}{T_{s0}}d \tag{0.39}$$

Thus provided the effective length of the suspension is the same for lateral and rotational displacements the gyradius can be measured without measuring the suspension length *l* or knowing the precise value of "*g"*. Simple and bifilar pendula are subject to the buoyancy force due to the surrounding air and this is normally taken into account by modifying the value of "g" in equations(0.1) and (0.57). However, both the variation of "*g"* with latitude and this correction cancel in the period ratio, as does any calibration error in the timer. The effects of added mass[58,59] may also partially cancel.

If both oscillations are simultaneously excited a point outside the plane of the suspension can be observed to have a beat pattern. The ratio of the periods can then be deduced from "*n"* the number of oscillations per beat, as:

$$n=\frac{T_{beat}}{T_{average}}=\frac{\left(T_y/T_s+1\right)}{2\left(T_y/T_s-1\right)}\quad or\quad\frac{\left(T_s/T_y+1\right)}{2\left(T_s/T_y-1\right)} \tag{0.40}$$

Depending on if $T_y>T_s$ or $T_y<T_s$. So

$$k_y=\frac{T_y}{T_s}d=\frac{2n+1}{2n-1}d\quad or\quad\frac{2n-1}{2n+1}d \tag{0.41}$$

Depending on whether $k_y>d$ or $k_y<d$. This ambiguity can be resolved using equation(0.39) or by changing *d*.

The number *n* can be determined by patient observation of the motion, so only a ruler is required to measure the spacing 2*d*. Even the suspension only has to be

approximately parallel if $2d$ is measured as the geometric mean spacing[14],[60]. By choosing the spacing d to be close to the gyradius n becomes large and this estimate of k_y can be quite precise. A further advantage of choosing the spacing close to the gyradius is that any mass added at the ends of the suspension lines due to bearings etc. has only a minor effect on the measurement so any correction need only be known approximately.

One caveat, for separate displacements in the plane of the suspension, and for rotations about the symmetry axis the suspended object remains level. However, for combined lateral and rotational displacement together, the support lines no longer make equal angles ϕ_1 and ϕ_2, with the vertical, and so there is some rotation about the horizontal axes, which therefore have to be included in the Lagrangian. For small rotations of suspensions with $l >> d$ this effect is negligible. However, for suspension lengths such that the period T_y of yaw oscillation is close to that of one of the normal mode periods of the double pendulum pitch oscillations in the x-z plane, this term leads to a fascinating coupled oscillation[16] reminiscent of a Wilberforce pendulum[61]. The double pendulum mode splits into two frequencies and the initial Yaw-sway oscillation transforms into a beating pitch oscillation, i.e. rotation about the axis B-D, then back to a yaw-sway oscillation about the z axis, and so on. When close to this resonant condition the period of yaw oscillation is no longer precisely that given by equation(0.38). However, this motion does not occur for pure sway or pure yaw displacements so separate measurements of the periods T_y and T_s can still be made to determine the yaw gyradius k_y. To avoid this motion measurement or calculation of the periods of the two normal modes of the double pendulum motion can easily be made and the geometry adjusted accordingly. Such double pendulum data can also be used to determine the pitch gyradius k_p about the y axis, and the depth "a" of the center of mass below the line B-D[62].

G. Yaw Oscillation period, massless lines, Integral approach

The period of un-damped large amplitude yaw oscillation of a bifilar suspension can similarly be derived from equation(0.31) which, describes the motion in phase space, and as expected, leads to $\dot{\theta}_{Max} \approx \left(2\pi/T_{y0}\right)\theta_0$ for small θ_0. Although the following theory is derived for a bifilar suspension it also applies to the period of yaw oscillation of trifilar suspensions which have the advantage that the roll and pitch degrees of freedom are eliminated.

The yaw oscillation period is then given by:

$$T_y\left(\theta_0\right) = \frac{\varepsilon T_{y0}}{\pi\sqrt{2}} \int_0^{\theta_0} \frac{\sqrt{1-\varepsilon^2 Sin^2\left(\theta/2\right)\left[1-\kappa^{-2}Cos^2\left(\theta/2\right)\right]}}{\sqrt{\left\{\sqrt{1-\varepsilon^2 Sin^2\left(\theta/2\right)}-\sqrt{1-\varepsilon^2 Sin^2\left(\theta_0/2\right)}\right\}\left\{1-\varepsilon^2 Sin^2\left(\theta/2\right)\right\}}} d\theta \qquad (0.42)$$

Cromer[14] has treated the case for κ^{-2}<<1, i.e. neglecting the contribution of the vertical motion to the kinetic energy, which is the source of the squared bracket. The variation of the yaw period with amplitude then only depends on ε^2 and not on κ^2. For ε^2<<1 the integral can be expanded to give:

$$\begin{aligned}
\frac{T_y\left(\theta_0\right)}{T_{y0}} &\approx \frac{2}{\pi}\left\{K\left(k\right)-\frac{1}{8}\varepsilon^2 k^2\left(K\left(k\right)+\int_0^{\pi/2}\frac{Sin^2\varphi}{\sqrt{1-k^2Sin^2\varphi}}\,d\varphi\right)\right\} \\
&\approx \frac{2}{\pi}\left\{K\left(k\right)-\frac{1}{8}\varepsilon^2 k^2\left(K\left(k\right)+\frac{\left(K\left(k\right)-E\left(k\right)\right)}{k^2}\right)\right\} \\
&\approx \frac{2}{\pi}\left\{K\left(k\right)-\frac{1}{8}\varepsilon^2\left(\left(1+k^2\right)K\left(k\right)-E\left(k\right)\right)\right\} \\
\frac{T_y\left(\theta_0\right)}{T_{y0}} &= \frac{1}{M\left(\sqrt{1-k^2},1\right)}\left[1-\frac{\varepsilon^2\left\{1+k^2-N\left(1-k^2,1\right)\right\}}{8}-....\right]
\end{aligned} \qquad (0.43)$$

Where *E(k)* is the elliptical integral of the second kind[42], which can be rapidly evaluated using the Modified Arithmetic-Geometric Mean[46] *N(x,1)* as

$$E\left(k\right) = \int_0^{\pi/2}\sqrt{1-k^2Sin^2\theta}\;d\theta = \frac{\pi}{2}\frac{N\left(1-k^2,1\right)}{M\left(\sqrt{1-k^2},1\right)} \qquad (0.44)$$

It is interesting to note that for ε^2<1 the ratio $T_y(\theta)/T_s(\phi)$ of the yaw period to the sway period, for equal angular displacements, remains essentially independent of the

amplitude, thus simple gyradius measurements can be made with relatively large amplitude oscillations.

For small angles θ_0<<1 this can be further approximated to:

$$T_y(\theta_0)/T_{y0} \approx 1+\left(4-3\varepsilon^2\right)\theta_0^2/64 \tag{0.45}$$

Which should be compared with equation(0.55). However, for κ^2~1 and ε^2~1 the vertical kinetic energy can no longer be ignored. The vertical and rotational contributions to the kinetic energy have different θ dependence, so the variation of the period with amplitude then depends on both κ^2 and ε^2. The yaw period should therefore be calculated from equation(0.42) or numerical solutions of equation(0.34).

H. Rotational Yaw Oscillation, including finite mass suspension lines

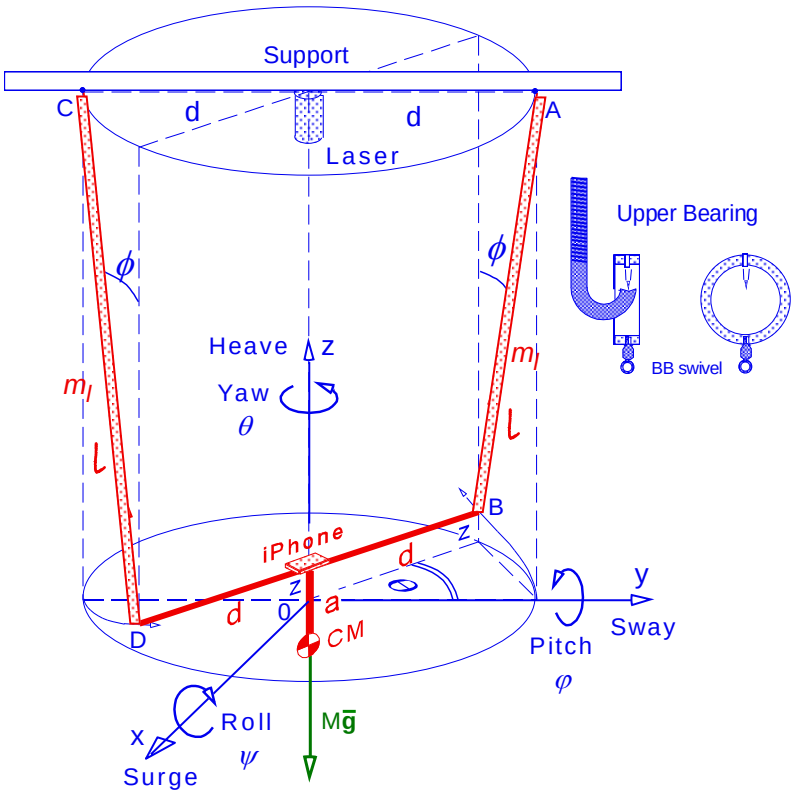

Figure 4 *Rotation about the vertical symmetry axis of a parallel bifilar suspension, with suspension lines mass m_l, spacing 2d and length l, of a body of mass M with its center of mass a distance "a" below the center of the suspension points B-D.*

For rotation about the symmetry axis, of a body with $b = 0$, convenient generalized coordinates are θ, the angle of yaw rotation about the z axis, the roll angle $\varphi = 0$, and the coordinates of the center of mass $x = y = 0$. The vector A-B representing the suspension line is $\vec{l} = \left(-d\,\mathrm{Sin}\,\theta,\ -d\left(1-\mathrm{Cos}\,\theta\right),\ -l\sqrt{1-\varepsilon^2\,\mathrm{Sin}^2\left(\theta/2\right)} \right)$ so the vertical displacement z of the ends of the lines, and the center of mass, when the suspension is rotated about the symmetry axis by an angle θ, see figure 1, is:

$$z = l - \sqrt{l^2 - 2d^2\left(1-cos\theta\right)} = l\left\{1-\sqrt{1-\varepsilon^2 sin^2\left(\theta/2\right)}\right\} \approx \left(\frac{d^2}{2l}\right)\theta^2 + \ldots \qquad (0.46)$$

Then the vertical velocity and acceleration are:

$$|\dot{z}| = \left(\frac{d^2}{l}\right)\frac{sin\theta}{\sqrt{1-\varepsilon^2 sin^2\left(\theta/2\right)}}\dot{\theta} = \frac{d\varepsilon\ sin\left(\theta/2\right)\cos\left(\theta/2\right)}{\sqrt{1-\varepsilon^2 sin^2\left(\theta/2\right)}}\dot{\theta} \qquad (0.47)$$

$$|\ddot{z}| = \left(\frac{d^2}{l}\right)\left[\frac{sin\theta}{\sqrt{1-\varepsilon^2 sin^2(\theta/2)}}\ddot{\theta} + \frac{\{cos\theta + \varepsilon^2 sin^4(\theta/2)\}}{\{1-\varepsilon^2 sin^2(\theta/2)\}^{3/2}}\dot{\theta}^2\right] \tag{0.48}$$

The square of the velocity of a point a fraction ξ along the suspension line from A, is:

$$v^2(\xi) = \frac{\varepsilon^2\{1-\varepsilon^2 Sin^4(\theta/2)\}}{4\{1-\varepsilon^2 Sin^2(\theta/2)\}}(\xi l)^2\dot{\theta}^2 \tag{0.49}$$

The Potential U_l and kinetic T_l energies for two lines of uniform linear density $\rho = m_l/l$ are:

$$U_l = m_l\, g\, l\sqrt{1-\varepsilon^2\,\mathrm{Sin}^2(\theta/2)} \qquad T_l = 2\int_0^l \frac{1}{2}\rho v^2(\xi)\,dl = \frac{m_l d^2\{1-\varepsilon^2 Sin^4(\theta/2)\}}{3\{1-\varepsilon^2 Sin^2(\theta/2)\}}\dot{\theta}^2 \tag{0.50}$$

So the total potential and kinetic energies in terms of $\lambda = m_l/M$ are:

$$U = M(1+\lambda)gl\left(1-\sqrt{1-\varepsilon^2 Sin^2(\theta/2)}\right) \tag{0.51}$$

$$T = \frac{1}{2}M\left\{k_y^2 + \left(\frac{d^2\varepsilon^2 Sin^2\theta}{4\{1-\varepsilon^2 Sin^2(\theta/2)\}}\right) + \frac{2\lambda d^2\{1-\varepsilon^2 Sin^4(\theta/2)\}}{3\{1-\varepsilon^2 Sin^2(\theta/2)\}}\right\}\dot{\theta}^2 \tag{0.52}$$

Where the second and third terms are the kinetic energies due to the vertical motion and the suspension lines. Lagrange's equation[6] then leads to the nonlinear differential equation:

$$\left\{\frac{k_y^2}{d^2} + \frac{\varepsilon^2 Sin^2\theta}{4\{1-\varepsilon^2 Sin^2(\theta/2)\}} + \frac{2\lambda\{1-\varepsilon^2 Sin^4(\theta/2)\}}{3\{1-\varepsilon^2 Sin^2(\theta/2)\}}\right\}\ddot{\theta}$$
$$+\left\{\frac{Cos\theta + \varepsilon^2 Sin^4(\theta/2)}{4\{1-\varepsilon^2 Sin^2(\theta/2)\}^2} + \frac{\lambda\left[1-2Sin^2(\theta/2)+\varepsilon^2 Sin^4(\theta/2)\right]}{6\{1-\varepsilon^2 Sin^2(\theta/2)\}^2}\right\}\varepsilon^2 Sin\theta\dot{\theta}^2 \tag{0.53}$$
$$+\frac{g(1+\lambda)}{l\sqrt{1-\varepsilon^2 Sin^2(\theta/2)}}Sin\theta = 0$$

For λ = 0 and small angles θ << 1 equation (0.53) becomes:

$$\left\{1+\left(\frac{\varepsilon}{2\kappa}\right)^2\theta^2\right\}\ddot{\theta}-\left(\frac{\varepsilon}{2\kappa}\right)^2\theta\dot{\theta}^2\approx-\frac{g}{\kappa^2 l}\theta \tag{0.54}$$

And a trial solution[57] of the form $\theta(t)=\theta_0 Cos\left(2\pi t/T_y(\theta_0)\right)$ then leads to an amplitude dependent yaw period:

$$T_y(\theta_0)\approx 2\pi\kappa\sqrt{\frac{l}{g}}\left\{1+\frac{\theta_0^2}{16}\left(1-\frac{3\varepsilon^2}{4}+\frac{\varepsilon^2}{\kappa^2}\right)\right\} \tag{0.55}$$

For finite mass suspension lines, $\lambda \neq 0$ and ε << 1, equation(0.53) reduces to:

$$\left\{\frac{k_y^2}{d^2}+\frac{2\lambda}{3}\right\}\ddot{\theta}+\frac{g(1+\lambda)}{l}Sin\theta=0 \tag{0.56}$$

The small angle yaw period with finite λ is then:

$$T_{ym}=2\pi\left(\frac{k_y}{d}\right)\sqrt{\frac{l}{g}}\sqrt{\frac{1+2\lambda d^2/3k_y^2}{1+\lambda}} \tag{0.57}$$

Thus the period can be smaller or larger than the small angle λ = 0 period T_{yo}, depending on the spacing d and the gyradius k_y.

The yaw gyradius k_y can be determined in terms of the ratio of the small angle yaw and sway periods as:

$$k_y=d\left(\frac{T_{yo}}{T_{so}}\right)=d\left(\frac{T_{ym}}{T_{sm}}\right)\sqrt{\frac{(1+2\lambda/3)}{(1+2\lambda d^2/3k_y^2)}}=d\left(\frac{T_{ym}}{T_{sm}}\right)\sqrt{1+2\lambda\left(1-T_{sm}^2/T_{ym}^2\right)/3} \tag{0.58}$$

The correction to the gyradius for finite mass suspension lines cancels if $d = k_y$, i.e. $T_{ym} = T_{sm}$. This can easily be understood by picturing the body as a dumbbell with two $M/2$ masses separated by $2k_y$. Then, if the suspension spacing is $2d = 2k_y$, the small angle rotational oscillation is equivalent to two out of phase simple pendulums of periods equal to that of the in plane oscillation. The corrections for this simple pendulum motion perpendicular to the plane is identical to that for the in plane motion and therefore cancels.

I. Asymmetrical Bifilar Suspension Yaw

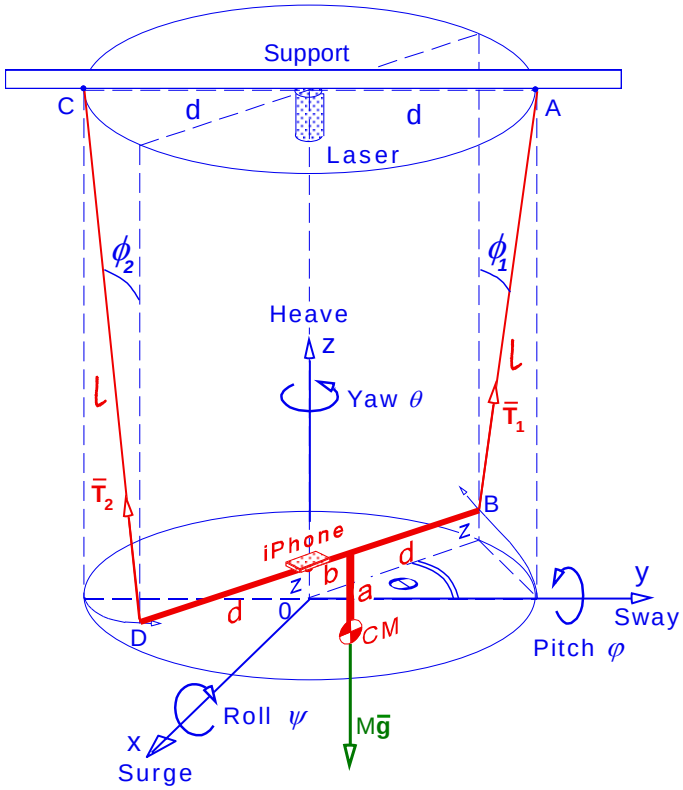

Figure 5 *Rotation about the vertical axis of a parallel bifilar suspension, with spacing 2d and length l, of a body of mass M with its center of mass a distance "b" from the symmetry axis and "a" below the center of the suspension points B-D.*

A bifilar suspension of a body for which the center of mass is not on the symmetry axis will, when released with yaw displacement θ, eventually develop motion in all the degrees of freedom. However, for small angular displacements the classical Newton's law treatment[15] provides an adequate basis for a derivation of the yaw oscillation period T_{yo}. Even in the accelerating frame of the suspended body the vertical torque Γ about the center of mass equals the yaw moment of inertia Mk_y^2 times the angular acceleration $\ddot{\theta}$. In equilibrium the suspension lines, now horizontally at *(d+b)* and *(d-b)* from the center of mass, see figure 5, have tensions of *Mg(d-b)/2d* and *Mg(d+b)/2d* respectively. For suspension lines of length "*l*" their horizontal components are $Mg(d-b)^2/ld\ Sin(\theta/2)$ and $Mg(d+b)^2/ld\ Sin(\theta/2)$ and are at angles $(\pi-\theta)/2$ to B-D. The torque Γ about the vertical axis through the center of mass is then $\Gamma = 2Mg\left(d^2-b^2\right)\sin\left(\theta/2\right)\cos\left(\left(\pi-\theta\right)/2\right)/l = Mk_y^2\ddot{\theta}$. Now approximating this for θ << 1

$$k_y^2\ddot{\theta} \approx \frac{gd^2\left(1-\left(b/d\right)^2\right)}{l}\theta \qquad (0.59)$$

This is the same as derived for a trifilar suspension by du Bois, Lieven and Adhikari[24] and is consistent with the formula given by Huw Williams[60]. Note that this analysis assumes the suspension is free to sway and surge and does not apply if a center pin is used to confine the yaw rotation to be about the symmetry axis, for which the parallel axis analysis would apply.
Then the yaw period, for a center of mass offset by b, is:

$$T_{yo} = \frac{2\pi k_y}{d}\sqrt{\frac{l}{g\left(1-\left(b/d\right)^2\right)}} = 2\pi k_y\sqrt{\frac{l}{g\left(d^2-b^2\right)}} \tag{0.60}$$

The yaw gyradius k_y is then given by:

$$k_y = \frac{T_{yo}}{2\pi}\sqrt{\frac{g\left(d^2-b^2\right)}{l}} = \frac{T_{yo}d}{T_{so}}\sqrt{1-\left(b/d\right)^2} \tag{0.61}$$

Where T_{so} is the small angle sway period which does not depend on either *d* or *b*.

J. Center of Mass location

The simplest way to determine the center of mass offset *b* from the symmetry axis of a bifilar suspension is to use strain gauges to measure the tensions T_1 and T_2 in the suspension lines. If however, strain gauges are not available other techniques can be used to correct asymmetrical suspensions and determine the position of the center of mass[63].

The off center distance *b* can be determined by symmetrically changing the suspension spacing *d* and then measuring the yaw period. Note that as *d* can be taken as approximately the geometric mean of the top and bottom spacing of non-parallel suspensions[14,64] it is sufficient to just change the suspension upper spacing, however, then one must avoid any sway as this will now engender roll.

Then with measured periods T_{y1} and T_{y2} for spacing d_1 and d_2:

$$k_y^2 = \frac{\left(d_1^2 - d_2^2\right) g {T_{y1}}^2 {T_{y2}}^2}{4\pi^2 l \left({T_{y2}}^2 - {T_{y1}}^2\right)} \qquad b^2 = \frac{\left(d_2^2 T_{y2}^2 - d_1^2 T_{y1}^2\right)}{\left(T_{y2}^2 - T_{y1}^2\right)} \tag{0.62}$$

Alternatively the yaw period T_{yo} has a minimum for $b = 0$ so determining this minimum as a function of the lateral displacement *y*, of the body relative to the symmetry axis, allows the position of the center of mass to be determined, see figure 14a. Rather than find the minimum, the body can be displaced a known distance "*e*" so *b* is increased to (*b*+*e*), and the period T_{ye} measured.

The distance *b* is then:

$$b = \sqrt{e^2 \left\{ \frac{T_{yo} T_{ye}}{T_{ye}^2 - T_{yo}^2} \right\}^2 + d^2} - e \left\{ \frac{T_{ye}^2}{T_{ye}^2 - T_{yo}^2} \right\} \tag{0.63}$$

Which can be inserted in equation(0.61) to calculate the corrected yaw gyradius.

K. Trifilar Suspension

The trifilar suspension has the advantage that it has only three degrees of freedom, namely yaw, sway and surge, thus both roll and pitch are eliminated, and is therefore commonly used for Moment of Inertia measurements about a vertical axis[11,65]. It is still, however, free to oscillate in sway and surge, which now both have the simple pendulum period T_{so}. Thus equation(0.39) also applies to the trifilar suspension and will similarly improve the precision of the measurements.

The major disadvantage is that for accurate gyradius measurement the center of mass of the body must be located on the symmetry axis and for large complex objects such as engine blocks[11] this is not a trivial task. It is usually achieved using strain gauges and adding additional masses until the tensions are equal, and then correcting for the added moment of inertia[11].

In general the object to be measured is placed on a symmetrical suspended tray, mass m_T and gyradius k_T, which have been previously determined. Equation(0.61), with d as the distance from the suspension lines to the symmetry axis, also applies to the trifilar suspension[24] and shows that the correction to the measured gyradius for misalignment is of order $(b/d)^2$ and therefore generally small[24].

The period of oscillation of an asymmetrical trifilar suspension with parallel suspension lines of equal length l at distances d_1, d_2, and d_3 from the center of mass of the suspended body, and with angles θ_1, θ_2, and θ_3 between them (angle θ_1, being opposite d_1 etc. see figure 6a) is quoted without proof by Huw Williams[60] but can be derived in a similar manner to equation(0.59) as:

$$T_{yo} = 2\pi k_y \sqrt{\frac{l}{g}} \sqrt{\frac{d_2 d_3 \operatorname{Sin}\theta_1 + d_3 d_1 \operatorname{Sin}\theta_2 + d_1 d_2 \operatorname{Sin}\theta_3}{d_1 d_2 d_3 \left(d_1 \operatorname{Sin}\theta_1 + d_2 \operatorname{Sin}\theta_2 + d_3 \operatorname{Sin}\theta_3\right)}} \qquad (0.64)$$

Which reduces to equation(0.60) for the center of mass offset by b from the symmetry axis of a trifilar suspension.

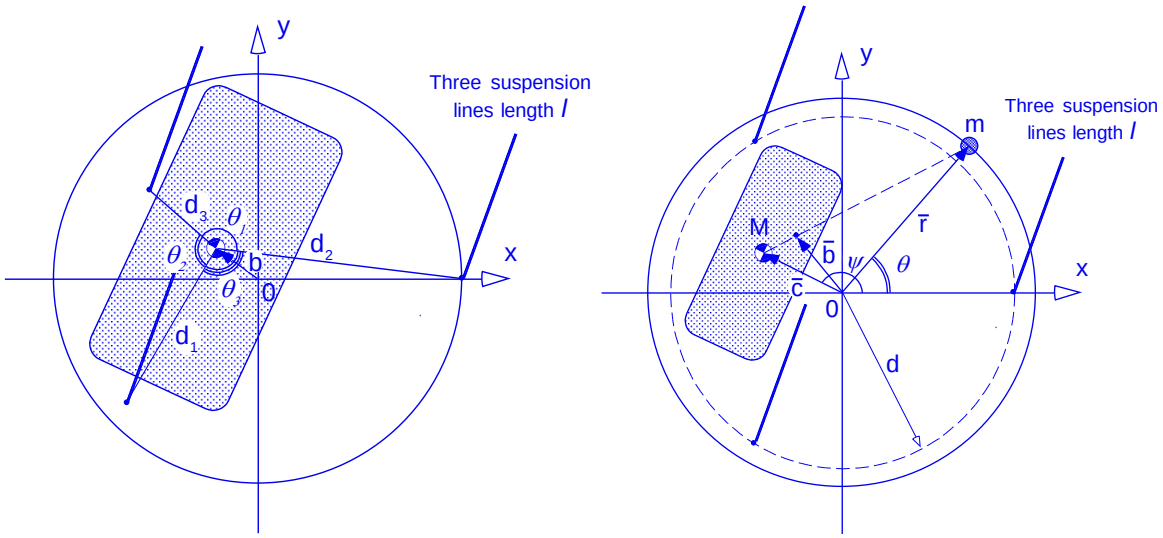

Figure 6 a) *A trifilar suspension with the "body plus tray" center of mass at distances d_1, d_2 and d_3 from the suspension points, see equation*(0.64). b) *A symmetrical trifilar suspension with a body mass M, gyradius k_y, center of mass of "body plus tray" at* ***c*** *from the symmetry axis and azimuthal angle ψ, plus a mass m, gyradius k_m, at radius r and azimuthal angle θ. The combined center of mass is then at* ***b****. The parallel suspension lines of length l are each at a radius d.*

In the absence of stain gauges, and where it is inconvenient to move the body on the tray the yaw period variation $T_{ym}(\theta)$ with the azimuthal angle θ of the added mass m, gyradius k_m, at constant radius r, can be used to determine the offset of the center of mass. For simplicity the tray, mass m_T, is combined with the body to be measured, mass M, so $M_T = M + m_T$, and the center of mass in figure 6 is that of the body plus tray, at c from the symmetry axis and azimuthal angle ψ. Then $m = \gamma (M + m_T)$. The mass m should

be chosen so that it will somewhat more than compensate for the estimated offset *c*. The combined center of mass is a distance *b* from the symmetry axis, given by:

$$b^2\left(1+\gamma\right)^2 = c^2 + \gamma^2 r^2 + 2\gamma rc\,\mathrm{Cos}\left(\psi-\theta\right) \tag{0.65}$$

The gyradius k_{cm} about the combined center of mass is then given by:

$$k_{cm}^2\left(1+\gamma\right) = \left(c^2 + k_{yT}^2\right) + \gamma\left(r^2 + k_m^2\right) - \left(1+\gamma\right)b^2 \tag{0.66}$$

Where k_{yT} is the gyradius of the tray plus offset body, and k_{cm} is the sum of the constant combined gyradius k_{mo} about the symmetry axis minus the parallel axis contribution, so:

$$k_{cm}^2 = k_{mo}^2 - b^2 \tag{0.67}$$

With

$$k_{mo}^2 = \frac{\left(c^2 + k_{yT}^2\right) + \gamma\left(r^2 + k_m^2\right)}{\left(1+\gamma\right)} \tag{0.68}$$

The yaw period variation with added mass *m* azimuthal angle θ is:

$$\frac{\partial T_{yn}}{\partial\theta} = \frac{T_{so}^2\gamma rc\left(k_{mo}^2 - d^2\right)}{T_{yn}\left(1+\gamma\right)^2\left(d^2 - b^2\right)^2}\,\mathrm{Sin}\left(\psi-\theta\right) \tag{0.69}$$

And, except for the special case of $k_{mo} = d$, for which there is no period variation, has extrema at $\theta = \psi$ and $(\psi+\pi)$. The yaw period will be a minimum at $\theta_m = (\psi+\pi)$ if $k_{mo} > d$, or a maximum if $k_{mo} < d$. Which is the case can be determined from an initial determination of k_y. Thus ψ can be determined from the variation of T_{yn} with θ, however, if $k_{mo} \approx d$ then the extrema will be shallow so *m* should be chosen to avoid this.

The maximum T_{yn+} and minimum T_{yn-} yaw periods are:

$$T_{yn\pm}^2 = T_{so}^2\,\frac{\left(\left\{\left(c^2 + k_{yT}^2\right) + \gamma\left(r^2 + k_m^2\right)\right\}\left(1+\gamma\right) - \left(c \pm \gamma r\right)^2\right)}{\left(d^2\left(1+\gamma\right)^2 - \left(c \pm \gamma r\right)^2\right)} \tag{0.70}$$

Then the value of the center of mass offset *c* is:

$$\begin{aligned} c &= \gamma r\left\{\sqrt{\beta^2 - 1 - \left(d^2/r^2\right)\left(1+\gamma\right)^2} - \left|\beta\right|\right\} \\ \beta &= \frac{T_{yn+}^2 + T_{yn-}^2 - 2T_{so}^2}{T_{yn+}^2 - T_{yn-}^2} \end{aligned} \tag{0.71}$$

Where the absolute value of β takes care of *d* being greater or smaller than k_{mo}. Then either this value of *c* can be used to correct the measured gyradius, or the mass *m* can be adjusted so that *b* = 0 by making $m = (M + m_T)c/r$.

For the special case of $k_{mo} = d$, for which there is no yaw period variation with θ, the gyradius k_{yT} is given by:

$$k_{yT}^2 = \frac{T_{yT}^2\left(\gamma d^2 - \gamma\left(r^2 + k_m^2\right)\right)}{\left(T_{yT}^2 - T_{so}^2\right)} \tag{0.72}$$

Where T_{yT} is the yaw period without the added mass and T_{so} is the sway period.

Once the value of the yaw gyradius k_{yT}, about the combined center of mass of the tray plus offset body, is known the yaw gyradius k_y of the body about its center of mass is:

$$k_y^2 = \left(1 + \frac{m_T}{M}\right)\left(k_{yT}^2 - \frac{m_T}{M}c^2\right) - \frac{m_T}{M}k_T^2 \tag{0.73}$$

An interesting variant of the trifilar suspension is one with five suspension lines arranged so as to restrict the motion to pure rotation about the central axis. This arrangement has been used for high precision laboratory moment of inertia and center of mass measurements[26,25]. The precision of the period measurements was a part in 10^5, leading to a moment of inertia measurement precision of better than 1 part in 10^4, and center of mass location of the order of 1μm.

It should be noted that for this suspension, and other multi-filar suspensions where a center pin is employed to restrict the rotational motion to be about the symmetry axis, equation(0.60) does not apply. In these cases the gyradius is that about the symmetry axis, i.e. $k_o^2 = k_y^2 + c^2$, which is the basis of the precision center of mass measurements.

L. Pitch-Surge Double Pendulum Oscillation

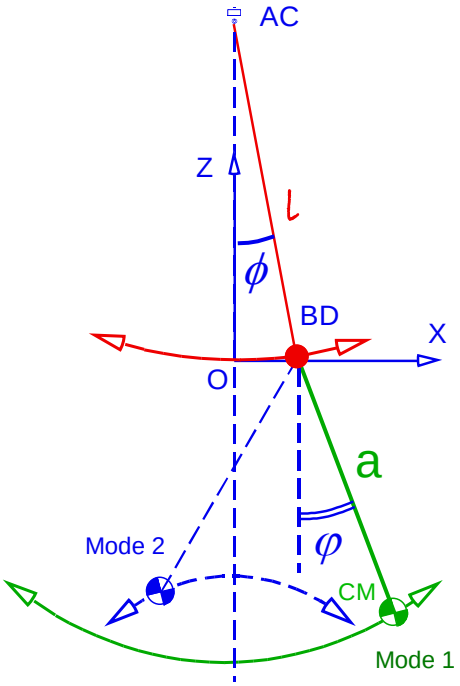

Figure 7 *A parallel bifilar suspension of length l, of a body with its center of mass a distance "a" below the center of the suspension displaced in the x-z plane for double pendulum pitch-surge-heave oscillation, with normal mode 1 in phase and mode 2 π out of phase.*

A bifilar suspension can be excited in pitch-surge double pendulum oscillation in the y-z plane perpendicular to the x-z plane of the suspension[66]. The appropriate general coordinates are ϕ, the angle the suspension lines make with the vertical, φ the pitch angle of the suspended body, the yaw and roll angles $\theta = \psi = 0$ or the sway displacement $y = 0$. The problem of the double pendulum has an interesting history[67]. The Emperor's bell (Kaiserglocke) of Cologne Cathedral was installed in 1885, but the bell did not ring reliably, as the clapper swung together with the bell in one of the normal modes. The problem was analyzed by Von Veltmann [68] and later by G. Hamel [69] and appropriate corrections applied.

The planar double pendulum is a nonlinear system with two degrees of freedom[14] and so for large angular displacements is a simple system exhibiting chaotic motion[70,71] . The dynamics of the extended body double pendulum have been analysed by Ohlhoff and Richter[72], Rafat et al[10] and Akerlof[73], with emphasis on the analysis of the quasi periodic and chaotic trajectories while the present analysis is limited to a linearized treatment of the small angle oscillations.

The kinetic and potential energies of a body of mass *M*, pitch gyradius k_p, about the y axis, with its center of mass a distance "***a"*** below the lower bearing B-D and suspended by lines of length *l*, as shown in figure 7, are

$$T = \frac{1}{2} M \left\{ l^2 \dot{\phi}^2 + \left(a^2 + k_p^2 \right) \dot{\varphi}^2 + 2l\, a\, \dot{\phi}\dot{\varphi} Cos(\phi - \dot{\varphi} \right\} \tag{0.74}$$

$$U = Mg \left\{ l\left(1 - Cos\ \phi\right) + a\left(1 - Cos\ \varphi\right) \right\} \tag{0.75}$$

Then in the absence of damping[74,75,6] the Lagrangian leads to the nonlinear differential equations

$$\begin{aligned} l\ \ddot{\phi} + a\ \ddot{\varphi} Cos(\phi - \varphi) + a\ \dot{\varphi}^2 Sin(\phi - \varphi) &= -gSin\ \phi \\ \left(a^2 + k_p^2 \right) \ddot{\varphi} + la\ \ddot{\phi} Cos(\phi - \varphi) + la\ \dot{\phi}^2 Sin(\phi - \varphi) &= -gaSin\ \varphi \end{aligned} \tag{0.76}$$

However, in the limit of small angles one can substitute sinusoidal oscillations into Lagrange's equations[74], which leads to a quadratic equation with solutions ω_1 and ω_2 for the angular frequencies of the two normal modes:

$$\omega_{1,2}^2 = \frac{g}{2lk_p^2} \left\{ \left(la + a^2 + k_p^2 \right) \pm \sqrt{\left\{ la + a^2 + k_p^2 \right\}^2 - 4lak_p^2} \right\} \tag{0.77}$$

For mode 1 the oscillation about B-D is in phase with the pendular oscillation about the suspension A-C, while in mode 2 they are out of phase by 180º, as shown in figure 7.

Then re arranging leads to the center of mass height "***a"***, and pitch gyradius k_p as:

$$\begin{aligned} a &= \frac{gl\left(\omega_1^2 + \omega_2^2\right) - g^2}{l\omega_1^2\omega_2^2} - l = g\left\{ \frac{\omega_1^2 + \omega_2^2 - \omega_s^2}{\omega_1^2\omega_2^2} - \frac{1}{\omega_s^2} \right\} \\ &= l\left(1 - \frac{\omega_s^2}{\omega_1^2} \right)\left(\frac{\omega_s^2}{\omega_2^2} - 1 \right) \end{aligned} \tag{0.78}$$

$$\begin{aligned} k_p &= \frac{g}{l\omega_1^2\omega_2^2} \sqrt{gl\left(\omega_1^2 + \omega_2^2\right) - l^2\omega_1^2\omega_2^2 - g^2} = \frac{g}{\omega_1^2\omega_2^2} \sqrt{\omega_1^2\omega_s^2 + \omega_2^2\omega_s^2 - \omega_1^2\omega_2^2 - \omega_s^4} \\ &= l\frac{\omega_s^2}{\omega_1\,\omega_1} \sqrt{\left(1 - \omega_s^2/\omega_1^2\right)\left(\omega_s^2/\omega_2^2 - 1\right)} \end{aligned} \tag{0.79}$$

Measurements of the frequencies $\omega_1 = 2\pi/T_1$, $\omega_2 = 2\pi/T_2$ and the sway $\omega_s = 2\pi/T_s$ allow both the vertical position "*a"* of the center of mass below the suspension points B-D and the pitch gyradius k_p to be determined from a single set of frequency ratios. If the suspension length is precisely measured then the gravitational acceleration *g*, together with buoyancy and latitude corrections, can be eliminated. Thus the yaw as well as the

pitch gyradius and center of mass height can be measured without changing the bifilar suspension, and all the elements of the inertia tensor can be measured if the body is subsequently tilted[17].

R. C. de Jong and J. A. Mulder[76,77] have described a method of measuring the pitch and yaw moments of inertia, as well as the product of inertia of a full sized aircraft, by simultaneously exciting the yaw and double pendulum oscillations and using statistical parameter estimation techniques to analyse the multi degree of freedom oscillation data, namely the x, y and z accelerations and the yaw, pitch and roll angular velocities. The knife edge bearings at the ends of their bifilar suspension did not facilitate sway motion, so this was kept to a minimum. As shown below similar measurements are now possible using MEMs gyros and accelerometers and then analysed using Simulink[20,12]. Thus the techniques described here, in which only specific modes of oscillation are separately excited, are a subset of their more general technique.

IV. Results

A. Sway Accelerations

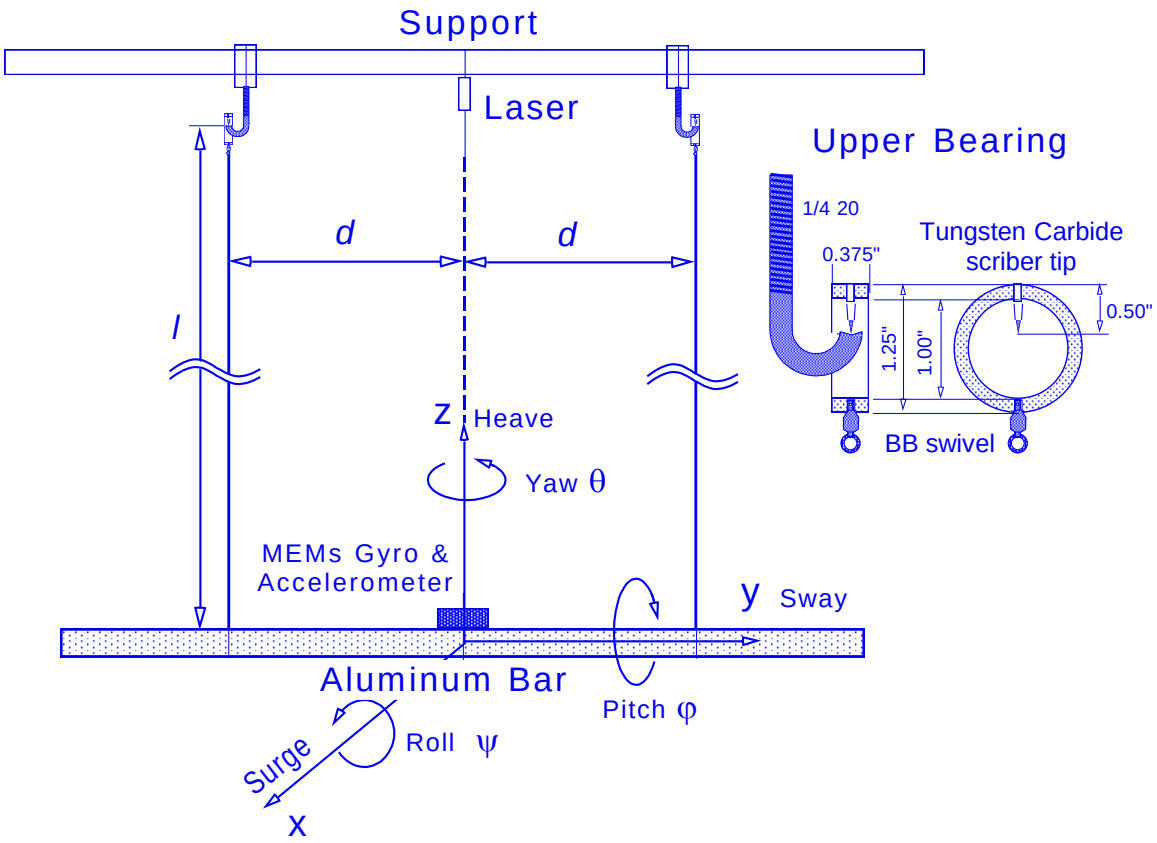

Figure 8 *The Aluminium bar and MEMs Gyro-accelerometer on the bifilar suspension of length l and spacing 2d. The inset shows details of the upper bearings.*

Two sets of acceleration measurements were made with a 1000 mm long aluminium bar of diameter 35.1 mm (2.615 kg) which was suspended by two light parallel lines (0.40 g/m) of effective length l = 1843 mm, and spaced at d = 289 mm from the center of the bar. The lines were tied to the bar and pivoted on tungsten carbide points at their upper ends, see figure 8. Thus $\alpha = a/d = 0.061$ and $\beta = b/d = 0$. A vertical laser beam on the symmetry axis provided a centering reference when releasing the bar, and scales below the suspension allowed the initial horizontal displacement to be determined.

The acceleration measurements were made with three instruments alternatively mounted at the center of the bar, an iPhone 4 with the xbow App[30], a Gulf Coast Data Concepts USB Accelerometer[29] Model X6-2, and a Micro Strain 3DM-GX1 Gyro Enhanced Orientation Sensor[31]. The GC X6-2 is a tri-axial accelerometer with no gyro but has the advantage of being light, battery powered and plugging into any USB port for subsequent data download. The iPhone has the advantage of being almost universally

available and has both tri-axial accelerometers, and three axis gyro outputs, but requires the up to 20 Meg xbow data files to be e-mailed for transfer to a computer, and is not drift compensated. The present data for the aluminium bar is that from the Micro Strain 3DM-GX1 which provided both three axis gyro and accelerometer outputs. The bar was displaced in the plane of the suspension at increments of 100 mm and the subsequent horizontal and vertical accelerations recorded at 40 samples per second with a resolution of ±0.001g.

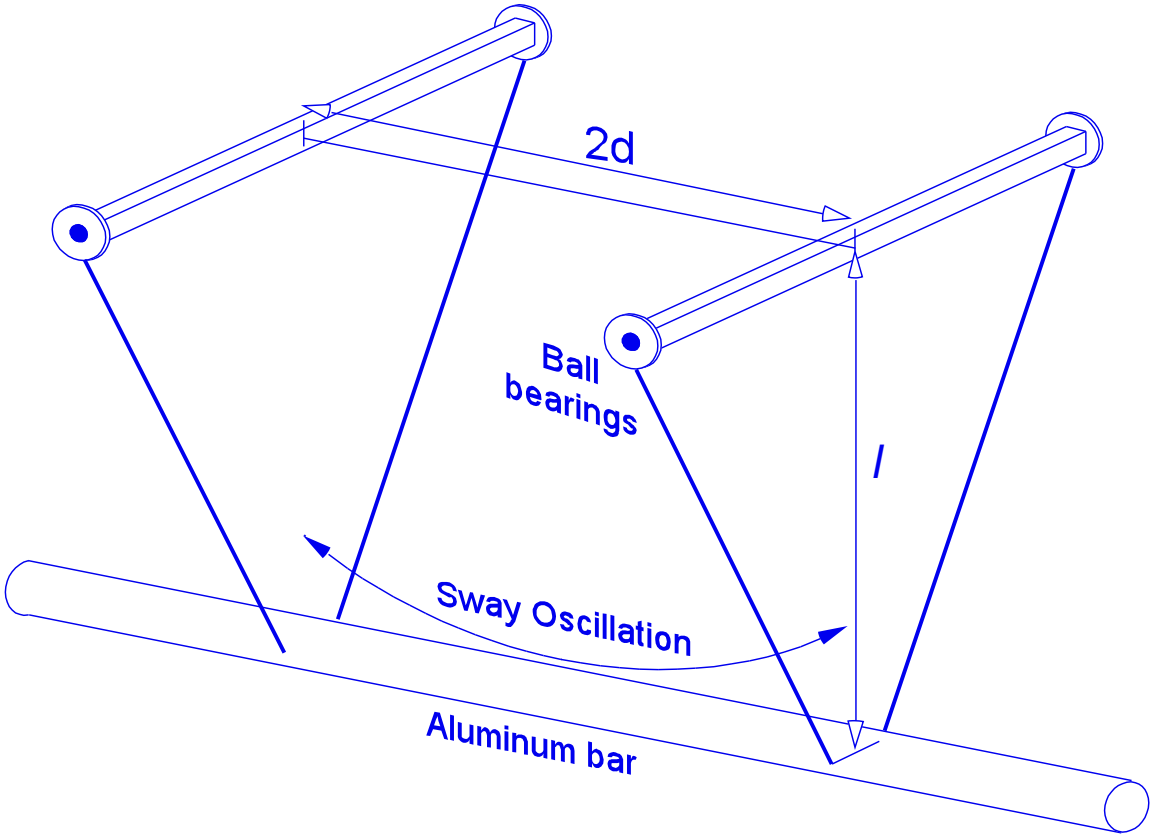

Figure 9 *The double "inverted V" suspension of effective length l = 463 mm, which prevented both yaw and surge motion. The upper bearings were ball bearings and the lower attachments to the aluminum bar were at the ends of diameters via holes in cable ties.*

Despite careful release and efforts to minimize the coupling to other modes of oscillation, the asymmetries and residual effects of the Micro Strain cable etc. led to surge and yaw which started to become significant after about 30 oscillations. Therefore in order to investigate the accelerations at larger angles, and also to confirm that the accelerations were independent of the pendulum length, a second set of data was recorded with the aluminium bar suspended by lines forming a double "inverted V" suspension, see figure 9, which prevented both yaw and surge motion, and was of effective length *l* = 463 mm.

The upper ends of the lines were attached to ball bearings, and the lower ends terminated approximately at the ends of a diameter of the bar, thus the center of mass height "a" was effectively zero. Plastic cable ties, with small holes at the ends of a

diameter, fastened the lines to the aluminum bar. The decrease of sway oscillation period at low amplitudes, see figure 18 is attributed to the ball bearings, as this effect has been observed with other ball bearing pendula[17].

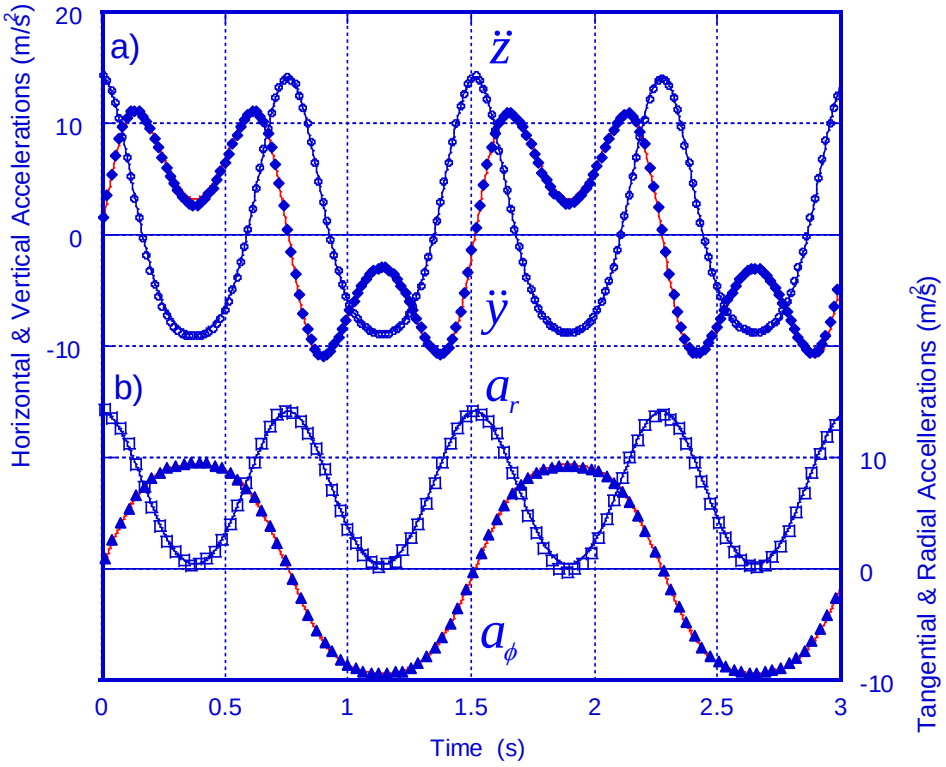

Figure 10 a) *The horizontal (solid diamonds) and vertical (open circles), and b) the tangential (solid triangles) and radial (open squares) accelerations as a function of time. The solid lines are a simultaneous fit to equations (4) with* $\phi(t) = \Sigma A_i Sin(2n_i\text{-}1)\omega_0 t$, *for* $\phi_0 = 1.29$ *radians* $= 73.8^0$ *and* $\omega_0 = 4.14\ s^{-1}$.

A typical large angle set of data from the “V” suspension, is shown in figure 10 and illustrates the non-sinusoidal nature of the large angle oscillations. The solid lines are a fits of equation(0.3) and(0.4) with $\phi(t)$ given by the first two terms of equation(0.22) i.e. $\phi(t) = \Sigma A_i Sin(2n_i\text{-}1)\omega_0 t$. The “Solver” routine in Excel was used to simultaneously minimize the squared deviations of 3 second data samples (at lower amplitudes 20 second samples were used) from both the $\ddot{y}$ and $\ddot{z}$ of equations(0.4) by varying only the period T and amplitude ϕ_0 (as well as the phase). Initial estimates of the period T_{so} and ϕ_0 can be obtained from equations(0.1) and(0.6), however, the latter depend on the zero offsets of the data which must therefore be eliminated prior to data analysis.

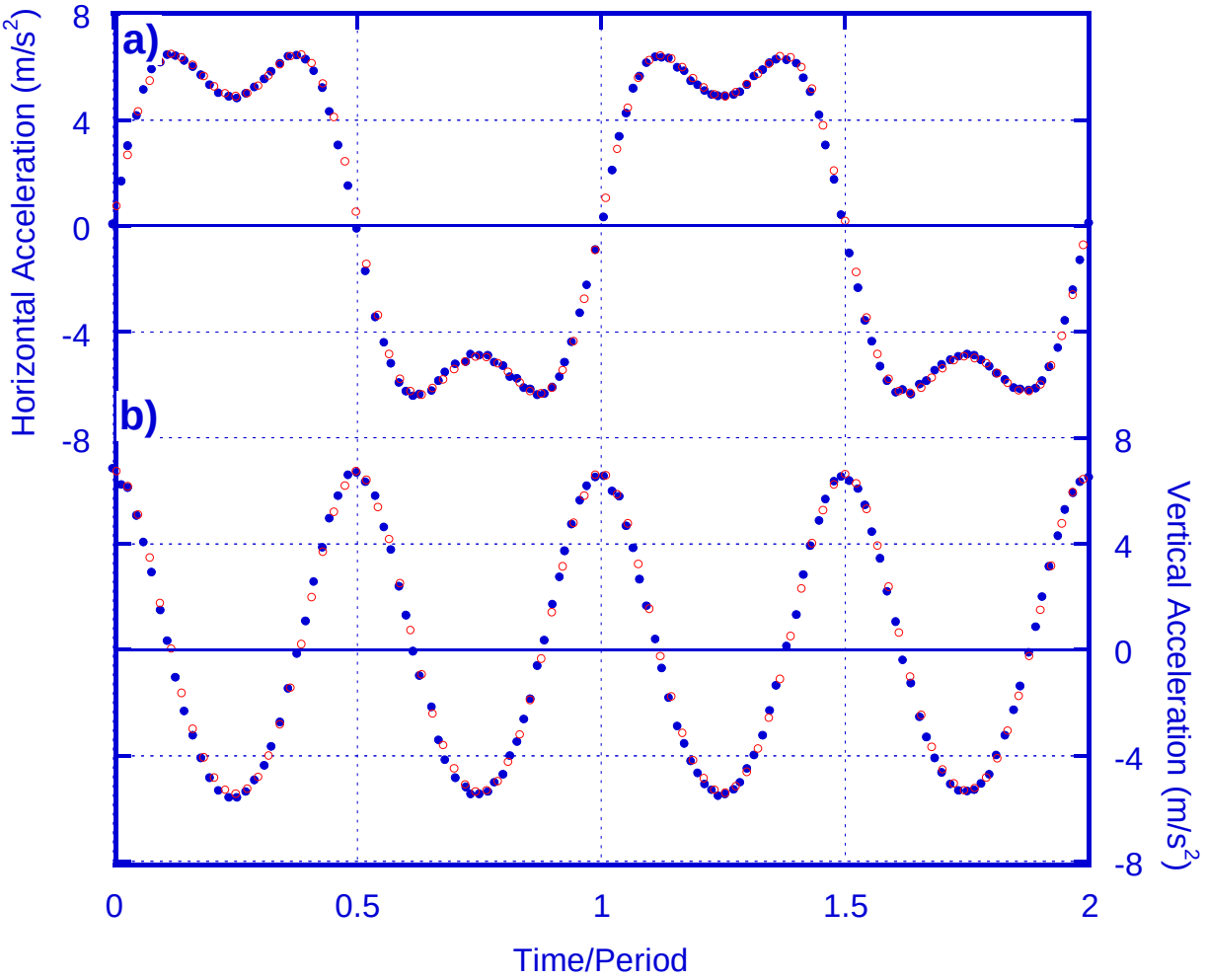

Figure 11 Comparison of a) *The horizontal and b) the vertical accelerations for* ϕ_0 *= 0.848 radians, as a function of time/Period. The solid circles are for the 1.843 mm suspension and the open circles are for the 463 mm "V" suspension.*

The fits of equation(0.4) to all the data taken with both systems and for amplitudes between 0.001 and 1.38 radians was excellent. Figure 11 shows a comparison of the 3DM-GX1 data for the 1843 mm suspension with the GC X6-2 data for the 463 mm "V" suspension, for equal amplitudes of ϕ_0 = 0.848 radians, after dividing the time scales by the oscillation periods. The agreement is such as to confirm that the accelerations are indeed independent of the pendulum length.

The deviations from sinusoidal of the angular oscillation, as derived using equation(0.5), indicated the presence of the third harmonic as predicted by equation(0.22) , see figure 12, and this was confirmed by a FFT. However, uncertainties in the zero offsets and the fits to the data made such analysis marginal, so a quantitative confirmation of equation(0.22) was not possible.

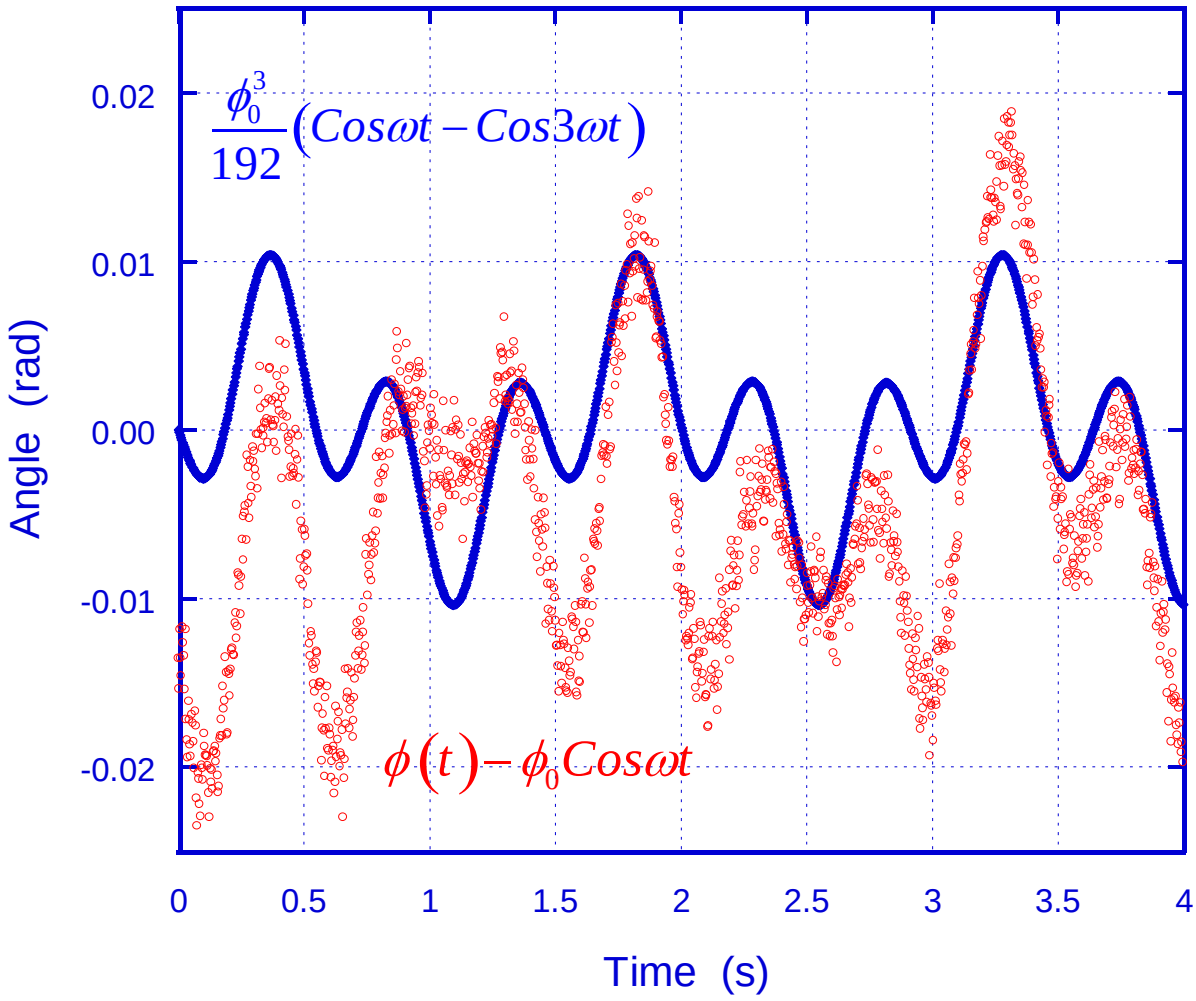

Figure 12 *The deviation of the angular displacement from sinusoidal (open circles) compared to the second term in equation*(0.22) *(closed circles). In this sample at* ϕ_0 *= 1.0 radians the third harmonic is clearly visible.*

B. Line Tensions for Sway Oscillation

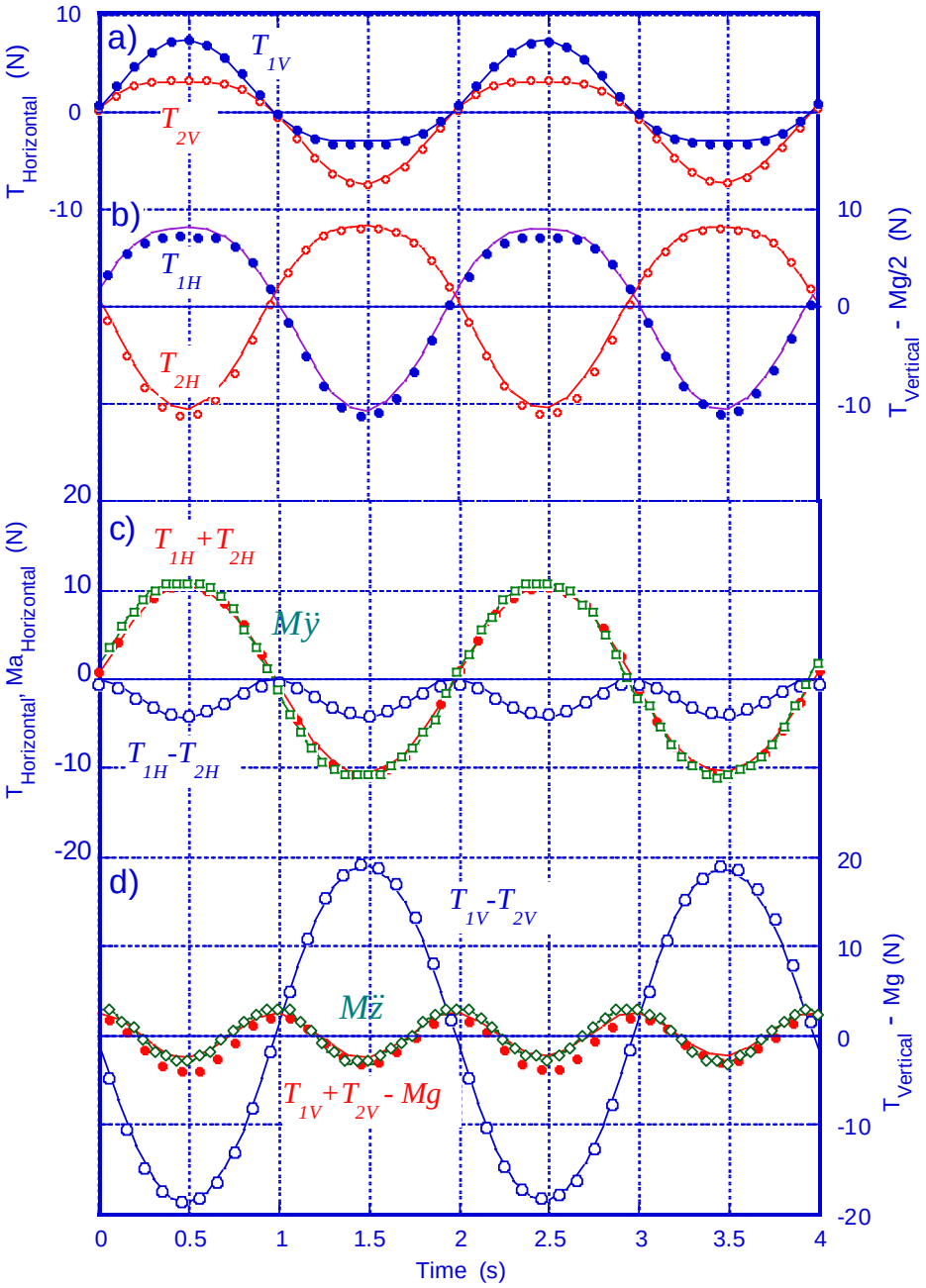

Figure 13 *The tensions T_1 and T_2 at a sway angular amplitude of 13.2° for a/d = 1.72 a) Horizontal components b) Vertical components minus Mg/2, c) The sum (solid circles), difference (open circles) of the horizontal components, and the mass times the horizontal acceleration (open squares). d) The sum minus Mg (solid circles) and difference (open circles) of the vertical components, and the mass times the vertical acceleration (open diamonds). The lines are a simultaneous fit of equation(0.14) to the four sets of data.*

In order to observe the effect of the depth $\alpha = a/d$ of the center of mass below the suspension points B-D on the tensions T_1 and T_2 a third set of data was taken with a wooden block (4.68 kg, 402 x 139 x 115 mm, with the 402 mm dimension vertical) attached to a light aluminium crossbar (241 x 9.5 x 4.8 mm). The parallel 965 mm long suspension lines were $2d$ = 230 mm apart, and pivoted on two fixed Vertical Pasco force gauges[78] which recorded the vertical components T_{1z} and T_{2z} of the tensions. An iPhone 4 was mounted on the block to record the sway accelerations. A second run with the force gauges horizontal, recorded the horizontal in y-z plane components T_{1y} and T_{2y} of the tensions. These two sets of data were synchronized using the iPhone 4 acceleration data, and then simultaneously fitted to equations(0.14), see figure 13.

The overall fit to the theory is very good except that the peak vertical components of T_1 and T_2 differed slightly. Careful measurements of the static tensions indicated that this was not due to any offset "b" of the center of mass, and is due to some instability of the force gauge zeros. Despite the significant differences in the tensions T_1 and T_2, see figure 13a and b, the horizontal and vertical components of their sum were in excellent agreement with the mass times the measured components of the acceleration, see figure 13c and d. The oscillation angular displacements, as derived from $\phi = A\tan\left(T_{Hi}/T_{Vi}\right)$ and from the horizontal acceleration were, as expected, also in good agreement. Finally the value of α = a/d = 1.7199 and β = b/d = 0.0003 derived from the fit to this data agreed with α = 1.72±0.01 and β = 0.00±0.01 deduced from the geometry of the block. Thus such data could be used to confirm the position of the center of mass.

C. Rotational Yaw Oscillation, finite mass suspension lines correction

A cylindrical wooden bar of length 1000 mm, diameter 35 mm and mass 489 gm was symmetrically suspended by two light cords (0.40 g/m) with point bearings at their upper ends, see figure 8. An iPhone 4 (115 x 58.6 x 9.5 mm, 140g) was mounted horizontally at the center of the wooden bar and recorded the angular and linear motions. The periods of sway and of yaw oscillation were measured for a suspension length l = 1686 mm at a number of line spacings d. These measurements were then repeated with 5 mm diameter copper beads strung onto the suspension lines (52.9 g/m).

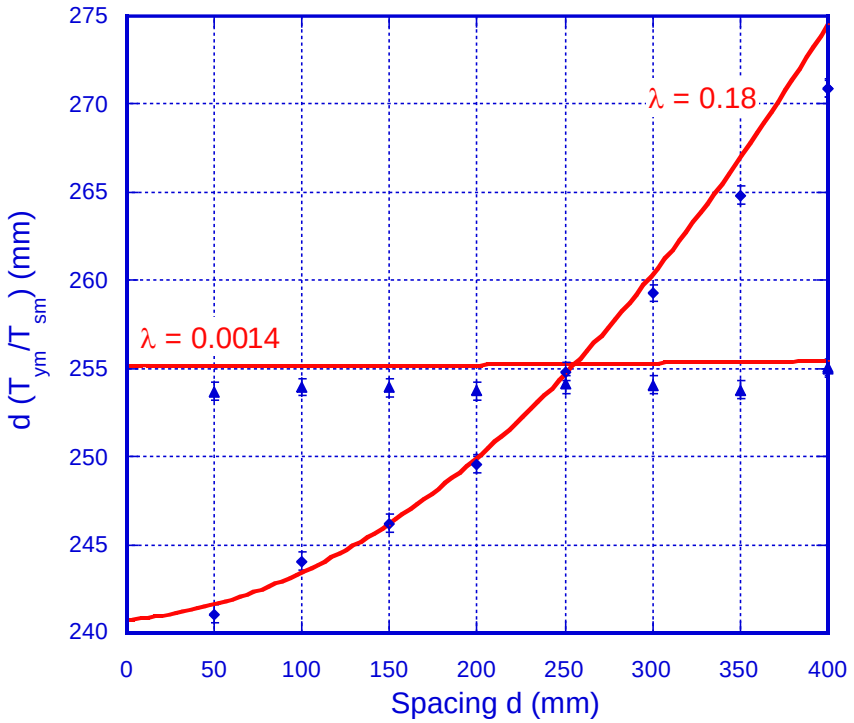

Figure 14 *The uncorrected gyradius* $k_y = d\left(T_{ym}/T_{sm}\right)$ *as a function of the line spacing d for the bare* $\lambda = 0.0014$*, and bead loaded lines* $\lambda = 0.18$*. The solid lines are the predictions of (24) with the theoretical gyradius of 255.3 mm.*

The sway oscillation periods T_{so} were, as expected, found to be independent of the spacing d, with the average of the 9 values being 2.608 ± 0.0006 s and 2.546 ± 0.001 s for $\lambda = m_l / M$ = 0.0014 and 0.18 respectively, compared to the predictions of equation(0.57) which, including a 7 mm change in the suspension length, were 2.605 ± 0.0015 and 2.533 ± 0.0015 s.

Figure 14 shows the uncorrected gyradius $k_y = d\left(T_{ym}/T_{sm}\right)$ as a function of the spacing d, for λ = 0.0014 and 0.18. The curves are the predictions of equation(0.57), with the theoretical gyradius of 255.3 mm, and demonstrate that for λ = 0.18 the correction can be significant but becomes zero for $d = k_y$.

D. Asymmetrical Bifilar Suspension Yaw Oscillation

Two sets of measurements were made with the aluminum bar and iPhone suspended by 1686 mm long lines. For the first set of data the spacing 2*d* was maintained at 500 mm and the center of the bar moved from b = 0 mm to 200 mm. For the second set one line was kept at 50 mm from the center and the other moved from 50 mm to 500 mm. The yaw periods, which varied from 3 to 14 seconds, were derived at amplitudes of 0.6 and 0.1 radians, and agreed after correction for the amplitude, thus suggesting that the effect of other oscillation modes on the yaw period were minimal. Figure 15a is a plot of the period times the spacing $T_y d$ versus the offset to spacing ratio b/d for both sets of data. Figure 15b is a plot of $l/g(2\pi/T_y d)^2$ versus $(b/d)^2$, which equation (0.60) predicts to be linear and the fit of $y = (1-x)/ k_y^2$ leads to k_y = 282.0 ± 0.2 mm as compared to a theoretical value of 281.8 mm.

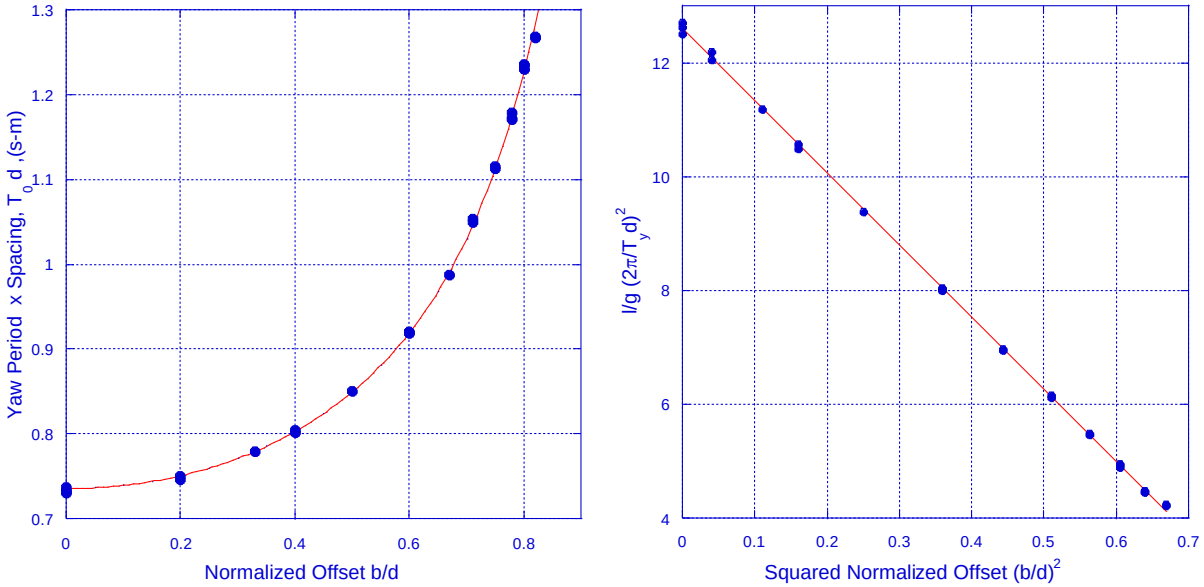

Figure 15 a) *The period times the spacing $T_0 d$ as a function of the ratio b/d of the CM offset b to the spacing d.* b) *A plot of $l/g(2\pi/T_y d)^2$ versus $(b/d)^2$. The lines are fits of* (0.60) *with k_y = 282.0 mm.*

Figure 16 shows the second set of yaw period data versus b/d together with equation (0.60) while figure 17 shows the yaw gyradius k_y as deduced from this data and demonstrates that the equation(0.61) is correct even for b/d = 0.8.

Table 1
Calculation of k_y and b from the periods at different spacing d

b(nominal)	d_1	d_2	T_{y1}	T_{y2}	k_y	b
150	250	200	3.6833	5.5670	282.8	149.9
150	250	200	3.6826	5.5741	282.4	150.2
100	250	150	3.2177	6.5805	283.2	99.7
100	250	150	3.2062	6.5852	281.8	100.4
50	250	100	3.0028	8.5029	282.3	50.2
50	250	100	2.9847	8.5035	280.3	51.2

As shown in table 1 the yaw gyradius k_y and center of mass offset *b* can be deduced from pairs of the data with different spacing d_1 and d_2 using equation(0.62), demonstrating that such measurements can be used to correct for any asymmetry in the suspension.

Alternatively equation(0.63) can be used to calculate the offset *b* from an added yaw period with the body displaced by a measured distance *e* and then this value of b can inserted into equation(0.61) to correct the gyradius measurement. Table 2 illustrates such an analysis of the present data.

Table 2
Calculation of the offset b from period measurements with a displacement e

b(nominal)	d	e	T_{y0}	T_{ye}	k_y	b
100	250	50	3.218	3.683	283.2	99.6
100	250	50	3.206	3.683	281.2	101.4
50	250	50	3.003	3.218	281.8	52.2
50	250	50	2.985	3.206	279.6	54.4

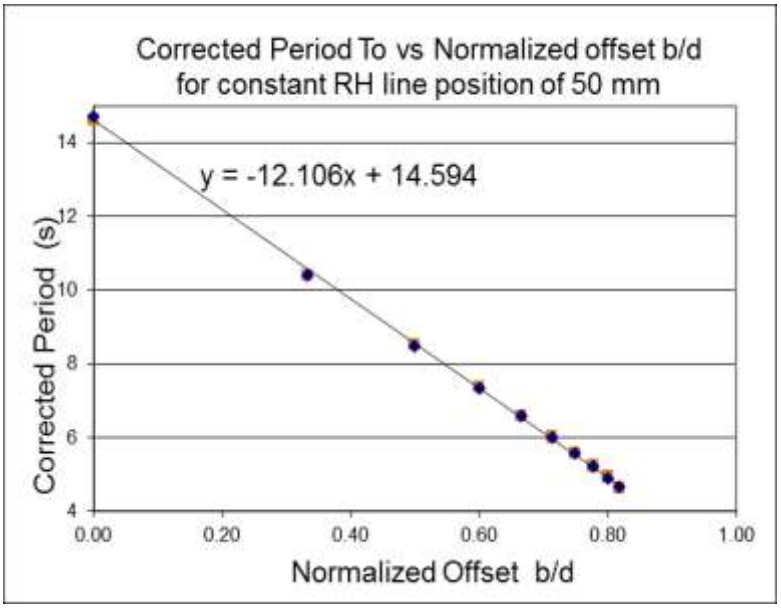

Figure 16 *The Normalized yaw period as a function of the ratio of the CM offset b to the spacing d. The offset b varied linearly with the spacing d. The square points are the theoretical prediction for* k_y *= 282 mm.*

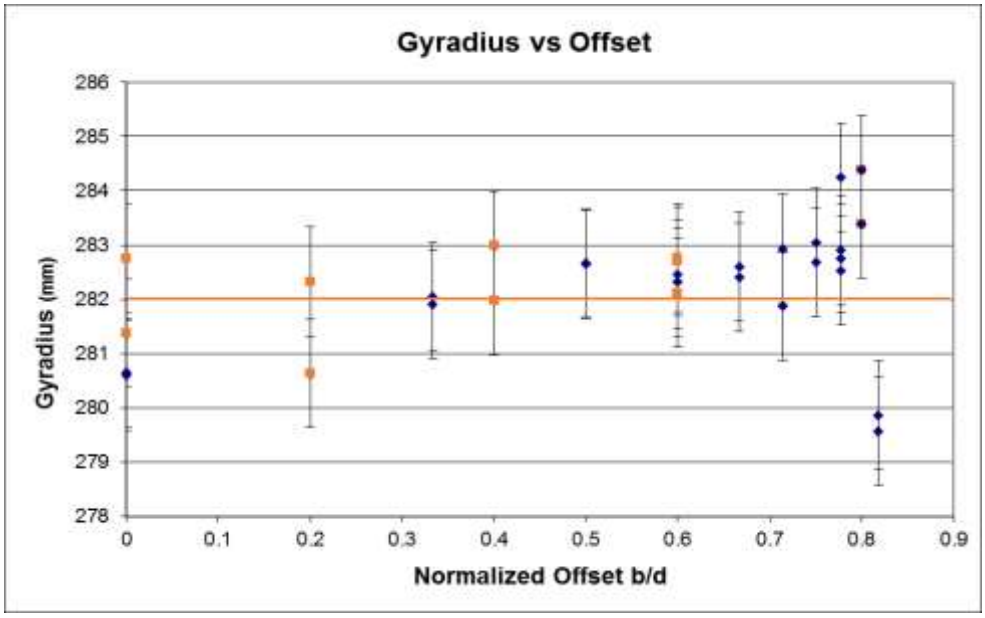

Figure 17 *The yaw gyradius as a function of the ratio of the CM offset b to the spacing d, for the two sets of data analysed at 0.1 and 0.6 radians and then corrected for amplitude.*

E. Sway Period Variation with Amplitude

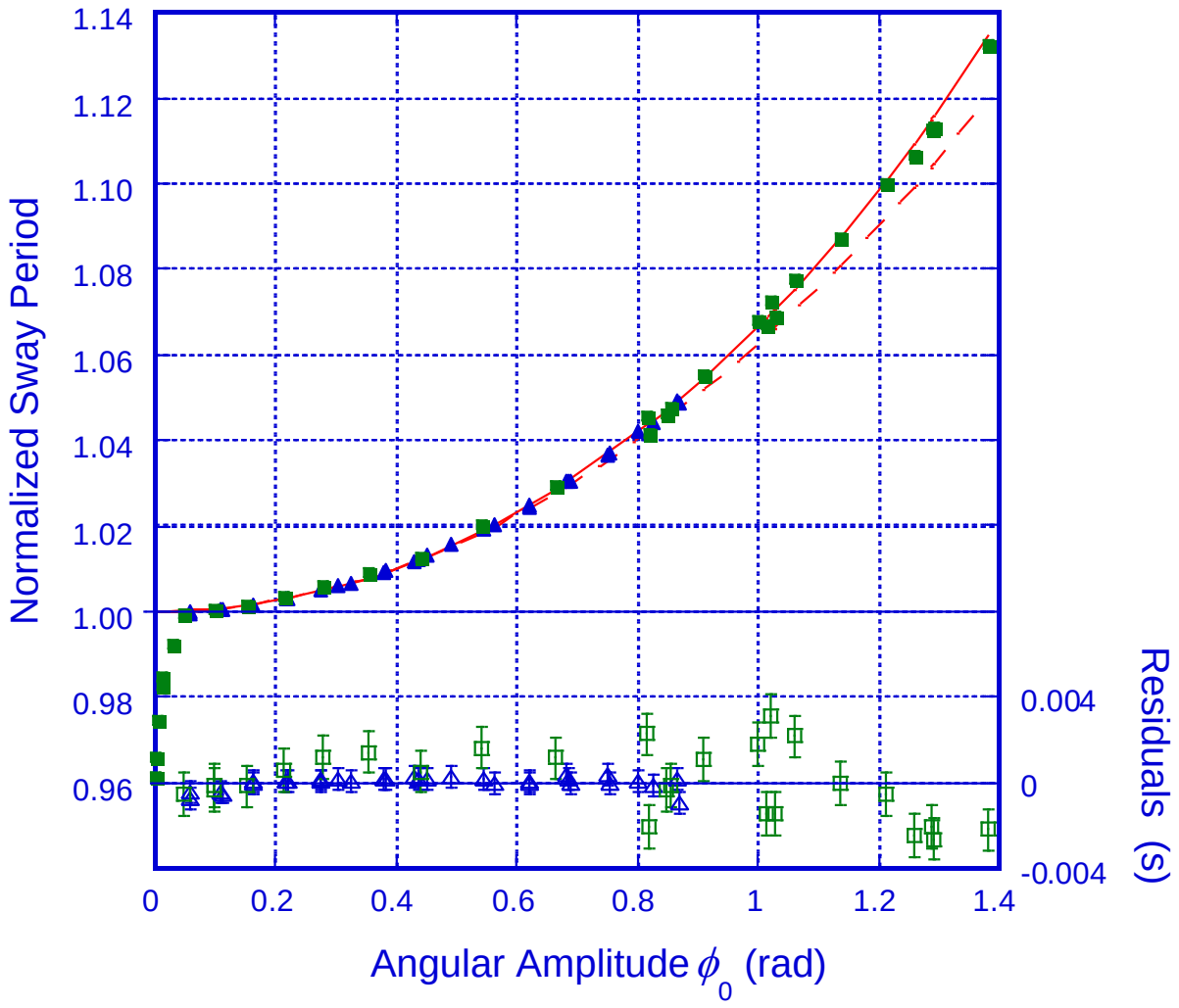

Figure 18 *The Period of sway oscillation as a function of the angular amplitude ϕ_0, as derived from a simultaneous fit to $\ddot{x}/g$ and $\ddot{z}/g$ data for the aluminium bar on an 1844 mm bifilar suspension (circles) and on a 463 mm "double inverted V" suspension (squares). The solid line is the Elliptic integral of the first kind, equation*(0.16), *while the dashed line shows only the first term of equation(0.17). The residuals from equation(0.16) for $\phi_0 > 0.03$ radians are shown below.*

The variation of the normalized period T_s/T_{s0} with sway angular amplitude ϕ_0 as derived from the fits to equations(0.4) is shown in figure 18, for both 20 second data samples for the 1844 mm suspension, and 3 second samples from the 463 mm "inverted V" suspension. The solid line is the elliptical integral of equation(0.16), then minimizing the deviations for $\phi_0 > 0.03$ radians, led to values of T_{s0} = 1.3634±0.0004s and 2.7295±0.0001s, which should be compared with T_{s0} = 1.365±0.003s and 2.725±0.003s

as derived from equation(0.1). The dashed line in figure 17 is for only the first term in equation (0.17) and demonstrates that the second term is clearly required above 0.8 radians. These results suggest that with sufficient attention to detail an inverted “V” bifilar pendulum can be used for precise measurements of the local acceleration due to gravity[13], without many of the corrections required for a classic pendulum[33].

The damping of the oscillation was observed to be non-exponential[33] but typically decayed by 1/e in 180 seconds so the effect on the period is expected to be negligible. The pronounced decrease in the period of the ball bearing “V” suspension at amplitudes below 0.04 radians, see figure 18, is ascribed to the effects of the bearings and is also observable, but to a much lesser extent, in the point bearing data. This effect has been observed in other measurements[17,79], makes extrapolation of small angle data problematical and deserves further investigation.

F. Yaw Period Variation with Amplitude

The aluminium bar, suspended by the two lines, was rotated through 180 degrees about the vertical symmetry axis, released, and the angular deflections and accelerations recorded by an iPhone[30] or the Micro Strain 3DM-GX1[31].The roll φ and pitch ψ rotations, as well as $\ddot{x}$ and $\ddot{y}$ accelerations, were monitored and found to be negligible, so the vertical acceleration $\ddot{z}$ could be studied as a function of the yaw angle $\theta(t)$, together with the variation of the oscillation period as a function of the amplitude θ_0.

A yaw angle of 180^0 is a point of unstable equilibrium so at yaw angles close to 180^o the torque is very small and it is therefore very difficult to determine the beginning of the motion, which is also very far from sinusoidal. Initially the damping is also significant so half oscillations, from zero to zero were analysed in terms of a Fourier series

$$\theta(t) = A_0 + \sum_1^7 A_{2n-1} Sin\left(2\pi(2n-1)(t-t_0)/T_y\right) \qquad (0.80)$$

The zero offset and drift of the instrument were first removed by fitting the absolute value of the data to a smooth envelope, and A_0 is included to account for any residual offset, while t_0 is the initial zero crossing of the half oscillation being analysed. The period T_y of the oscillation was then derived from a fit to the data using TableCurve 2D[80] and was confirmed by the differences between successive values of the zero crossing times t_i. Even with these corrections the initial damping was such as to decrease the amplitude sufficiently so as to change the period even during a half oscillation, thus the periods derived from data for amplitudes above 3 radians were not reliable.

The amplitude of the half oscillation as well as the time it occurred and the amplitudes $A_{(2n-1)}$ of the Fourier components were derived as a function of the amplitude θ_0. After the first 20 oscillations the quadratic damping had decreased significantly and so full oscillations and at low amplitudes up to 10 oscillations were analysed with the sum of the Fourier components curtailed at n = 3.

Table 3
Yaw period vs. Amplitude data

Suspension l (mm)	Spacing d (mm)	ε^2	κ^{-2}	T_{s0} (s)	T_{y0} (s)	k_y (mm)	*l(calc)* (mm)
1844	50	0.0029	0.031	2.721	15.044	276.3	1839
1820	150	0.0272	0.283	2.707	5.079	281.4	1820
1844	289	0.098	1.05		2.654	281.5	
1825	420	0.212	2.22	2.709	1.818	281.8	1824
204	50	0.240	0.031	0.909	5.083	280.4	205
1218	420	0.475	2.22	2.213	1.486	281.8	1217
1003	420	0.705	2.22	2.002	1.345	281.8	996

Although the primary variation of the yaw period is similar to that for the simple pendulum, the presence of ε^2 and κ^{-2} in equation(0.42) suggests that the large angle period depends somewhat on the geometry. Sets of 180^o Yaw data were therefore recorded for suspensions of the aluminium bar (k_y including the iPhone of 281.8 mm) with

the parameters listed in Table 3. The data is shown in figures 19, 20, 21 and 22, and confirmed a dependence of the large angle yaw period on both ε^2 and κ^{-2}.

The normalized yaw periods for $\varepsilon^2 = 0.098$, $\kappa^{-2} = 1.05$ and $\varepsilon^2 = 0.705$, $\kappa^{-2} = 2.22$ together with the theoretical curve for a simple pendulum, equation(0.16), are shown in figure 19. In order to see the data in more detail the deviations from equation(0.16) are shown as "Residuals" in figures 20 and 21, together with the theoretical values calculated from equation(0.34). The fits for large ε^2 shown in Figure 20 are good; however, those in figure 21 at smaller values of ε^2 leave something to be desired. For given κ^{-2} the Residuals at large angles are proportional to ε^2, and the value of θ_0 for zero residual is dependent on only κ^{-2}.

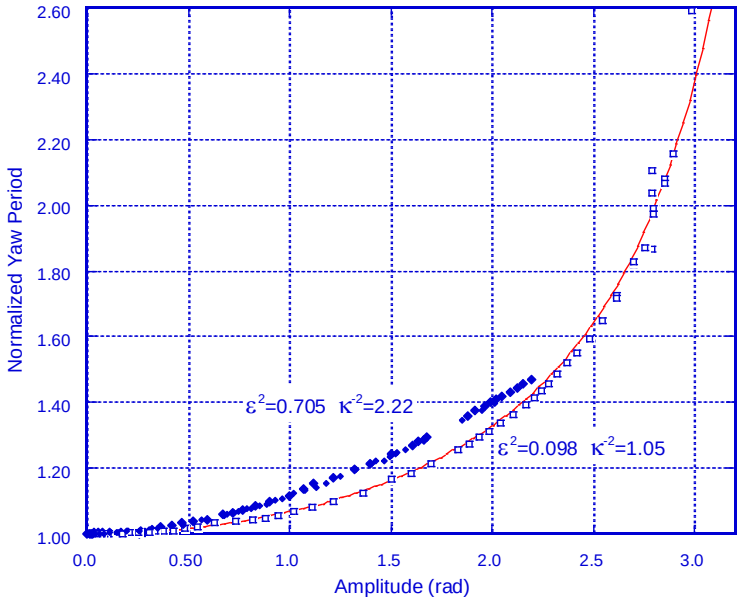

Figure 19 *The Normalized Periods of Yaw oscillation as a function of the angular amplitude θ_0, for an aluminium bar on a bifilar suspension with* $\varepsilon^2 = 0.098$ (open Squares) and $\varepsilon^2 = 0.705$ *(solid diamonds). The solid line is the elliptic integral equation(0.16).*

It should be pointed out that the damping at large angles was such that it could cause sufficient amplitude decrease during a single period so as to affect the results. So yaw period data for angles greater than 3 radians were rejected. It should also be pointed out that for geometries with large ε^2 it is difficult to excite pure yaw rotation, especially from an initial angle of π, as initially the suspension lines are essentially horizontal, and any parasitic sway modified the yaw period. A yaw-sway resonance for $\varepsilon^2 = 0.705$ and $\theta_0 \sim 1.8$ radians also significantly modulated the yaw periods as well as the amplitude decay.

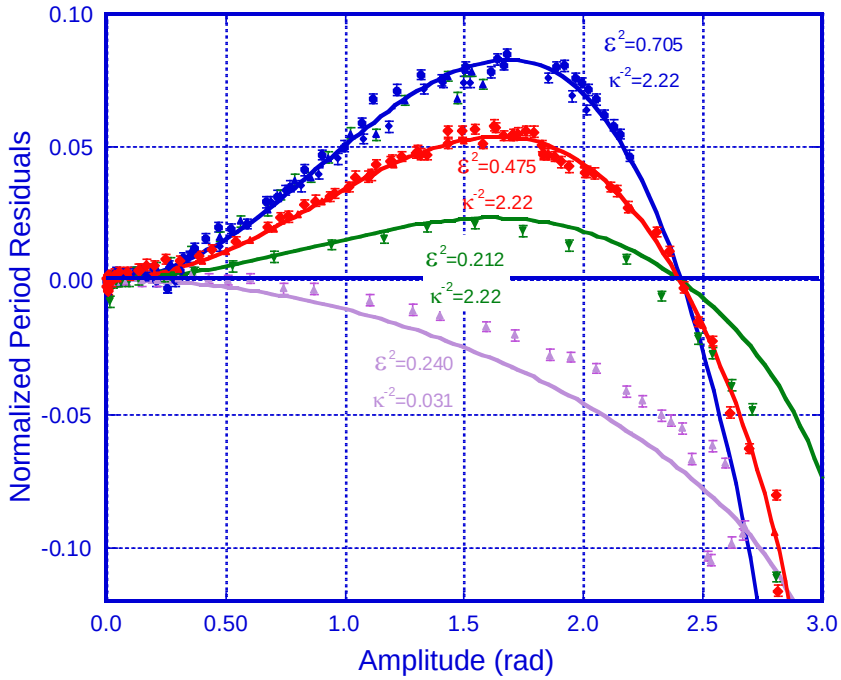

Figure 20 *The deviation of the Normalized Period of Yaw oscillation from equation(0.16) as a function of the angular amplitude θ_0 for large ε^2. . The solid lines are the theoretical predictions of equation(0.42).*

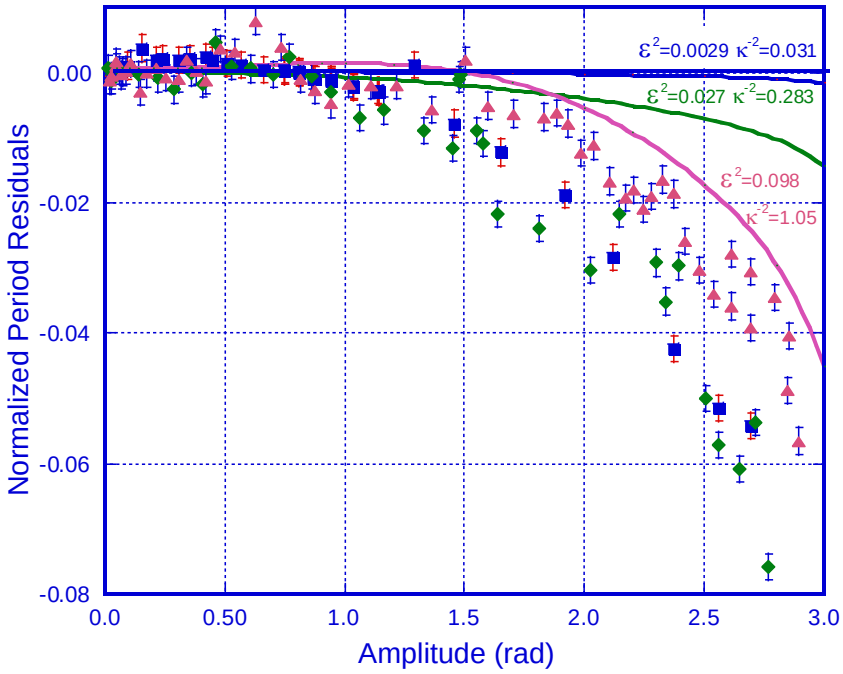

Figure 21 *The deviation of the Normalized Period of Yaw oscillation from equation(0.16) as a function of the angular amplitude θ_0 for small ε^2. The solid lines are the theoretical predictions of equation(0.42).*

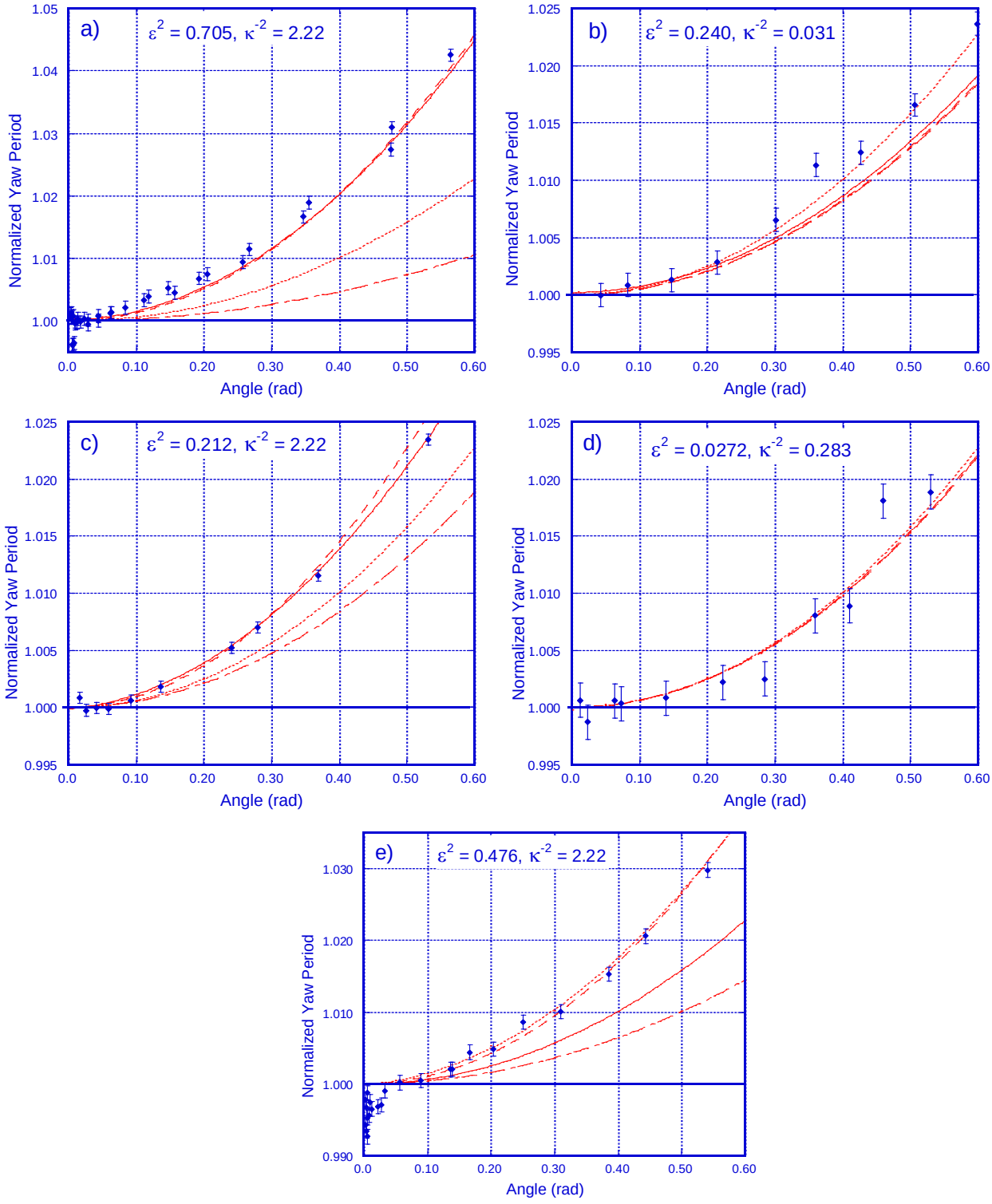

Figures 22 a to e *The Normalized Periods of Yaw oscillation as a function of the angular amplitude θ_0 for five suspensions. The periods for a simple pendulum equation (0.16) dotted line, the integral equation(0.42) solid line, the approximate equation (0.38) dashed line, and equation(0.45) dot dash line.*

Yaw gyradius measurements are generally made at small but not necessarily negligible amplitudes. At very low amplitudes bearing friction can significantly affect the period[79,17]. It was therefore of interest to compare the data for the simple pendulum period variation with amplitude, equation (0.16) with the integral equation (0.34) and the small angle approximation including the effect of the vertical motion, equation (0.38), and with equation (0.43)[14]. For amplitudes below 0.6 radians the approximate equation (0.38)was, as expected, in excellent agreement with the integral equation (0.34) and fitted all the data. For $\varepsilon^2 < 0.2$ all the equations were adequate, see figure 22a to d, however, for $\varepsilon^2 > 0.2$ the simple pendulum approximation, and for large κ^{-2} equation(0.43), are no longer adequate as the ratio of the average vertical KE to the angular KE is $\langle T_z / T_\theta \rangle_{ave} \approx \varepsilon^2 \kappa^{-2} \theta_0^2 / 16$.

Genta and Delprete[2] provide data on the variation of the period of a trifilar suspension with amplitude θ(rad), which is fitted $T/T_o = 1.00 + 0.121\ \theta^2$, i.e. double the variation predicted by equation(0.17) The suspension lines were not parallel so although the small angle period is approximately given by the geometric mean spacing[14,60], the variation of the period with amplitude may be quite different. However, with the data given[2] equation(0.55) suggests $T/T_o = 1.00 + 0.106\ \theta^2$ which is much closer than equation(0.17).

G. Variation of the Yaw Fourier components with Amplitude

At large angles the yaw displacement deviates significantly from sinusoidal and can be represented by a Fourier series of the odd harmonics as described by equation(0.80). The amplitudes of the Fourier components were extracted by least squares fitting single oscillations. The ratios of the Fourier components, A_3/A_1 and A_5/A_1, are shown as a function of the amplitude in figure 22. It should be noted that as Sine functions were fitted that A_3 is positive at large amplitudes, but for $\varepsilon^2 = 0.0029$, $\kappa^{-2} = 0.031$, contrary to theory, A_3 was negative below 1 radian.

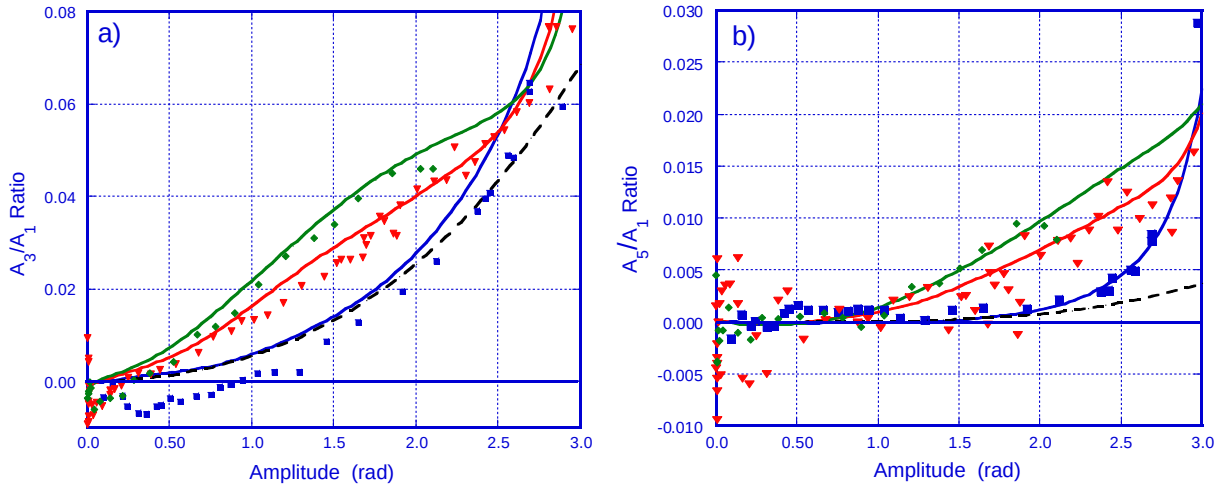

Figures 22 *The ratios of the amplitudes A_3 of the third and A_5 of the fifth harmonic to A_1 that of the fundamental as a function of the amplitude. Data for suspensions with $\varepsilon^2 = 0.705$, $\kappa^{-2} = 2.22$, diamonds, $\varepsilon^2 = 0.475$, $\kappa^{-2} = 2.22$, triangles and $\varepsilon^2 = 0.0029$, $\kappa^{-2} = 0.031$, squares. The solid lines are theoretical predictions based on equation(0.31) and the dashed line is equation(0.22).*

The theoretical curves shown in figure 23 were calculated by fitting equation(0.80) to four adjoined quarter period numerical solutions of equation*(0.31)* and are in generally good agreement with the data. The dashed curve in figure 23 is equation *(0.31)* for a simple pendulum. Figure 23 illustrates the significant dependence of A_3 and A_5 on the suspension parameters ε^2 and κ^2.

H. Yaw Large Angle phase space plots

Phase space plots for the simple pendulum are useful in understanding the details of the oscillations[35,81,82,83] and can be used to extract the inertia parameters independently of the damping[84]. At small amplitudes the plots of angular velocity versus angular displacement are ellipsoidal (i.e. SHM) but for initial angles θ_0 close to π they deviate significantly from ellipsoids. The deviations of the yaw oscillations of the bifilar pendulum from sinusoidal at large amplitude are also clearly illustrated by the phase space plots, as shown in figure 24, which shows samples of the data at amplitudes θ_0 of 0.5, 1.0, 1.5, 2.2 and 2.6 radians. The deviations from an elliptical shape are clearly more pronounced as ε^2 increases. The solid lines are the predictions of equation(0.31) for a) l = 1003mm, d = 421mm and b) l = 1844mm, d = 50mm with k_y = 281.8mm. The agreement is very good but small systematic deviations from the theory are evident and are presumably due to damping and small admixtures of other modes of oscillation. At small amplitudes the phase diagram is essentially elliptical but at amplitudes above 2 radians they deviate significantly from being ellipsoidal, and the shape depends on the parameters ε and κ of the suspension. The fit of equation(0.31) to the data depends critically on κ so this could be used to extract the yaw gyradius from large angle data.

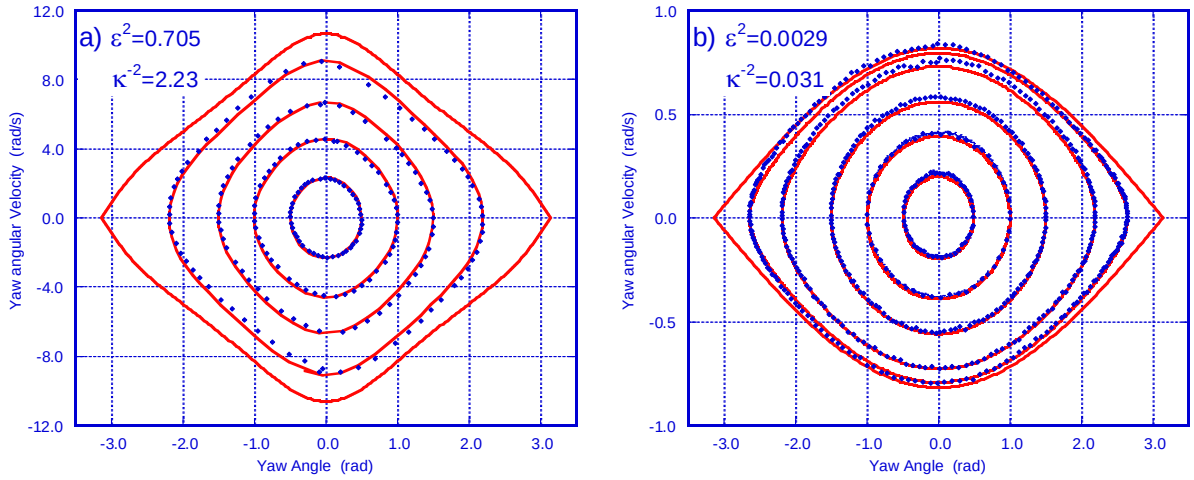

Figures 24 *The yaw angular velocity vs. angular displacement for suspensions with a)* $\varepsilon^2 = 0.705$ *and* $\kappa^{-2} = 2.23$ *and b)* $\varepsilon^2 = 0.0029$ *and* $\kappa^{-2} = 0.031$*(note the difference in angular velocity scales) for* $\theta_0 = 0.5, 1.0, 1.5, 2.2$ *and 2.6 radians. The solid lines are the predictions of equation(0.31) and include* $\theta_0 = \pi$ *for reference.*

I. Yaw Vertical Acceleration

Elementary treatments of bifilar yaw rotational oscillation[15] generally ignore the vertical dynamics, however, together with the yaw angle the iPhone records the vertical acceleration (in terms of "*g*" with a weight offset -1, which was therefore removed before comparison with theory). At small amplitudes the vertical acceleration is small and approximately sinusoidal; with a frequency double that of the yaw oscillation. However, as shown for large ε and amplitude θ_0 in figure 25, the vertical acceleration is significant, with a large maximum at the equilibrium position, which can exceed the saturation of the iPhone. Thus under these conditions the assumption[15] that the tensions are each *Mg*/2 is clearly no longer valid.

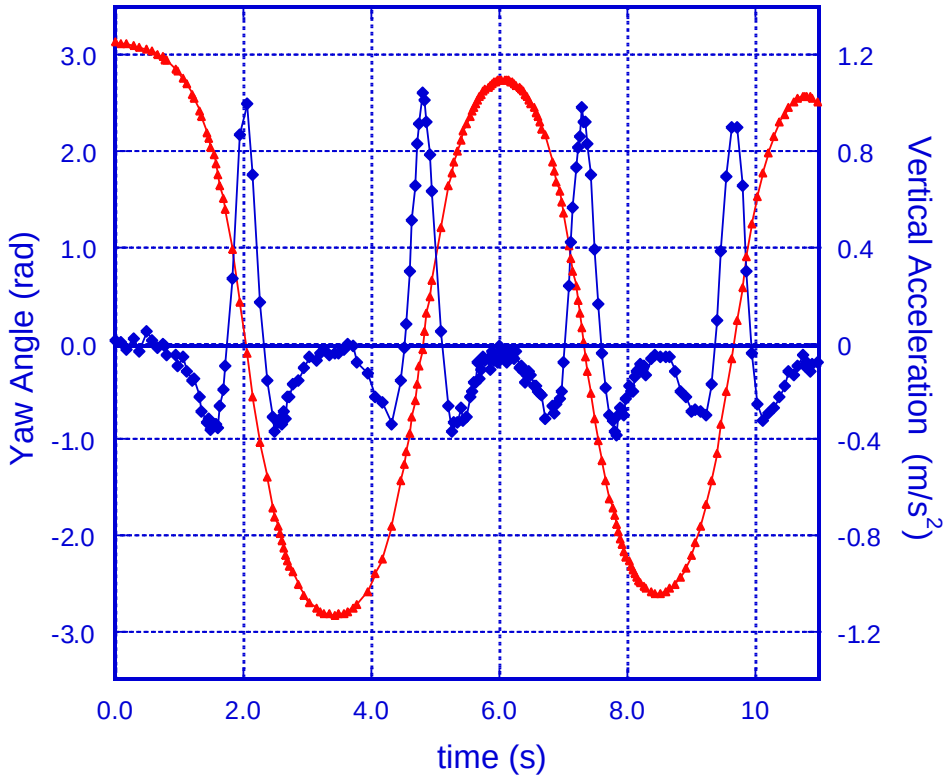

Figures 25 *The vertical acceleration data (diamond points) associated with large angle yaw oscillation (triangular points) versus time, for a bifilar suspension with* $\varepsilon^2 = 0.098$ *and* $\kappa^{-2} = 1.05$.

The vertical acceleration, see equation(0.27), has contributions dependent on the angular acceleration $\ddot{\theta}$ and on the square of the angular velocity $\dot{\theta}^2$. The leading term in the angular acceleration term is proportional to $Sin^2\theta$ and is therefore zero at the equilibrium position, but can have negative minima at angles less than the amplitude. The angular velocity term is zero at the amplitude θ_0 and has a maximum of $\ddot{z}_{Max} = 2gz_0/l\kappa^2$ at the equilibrium position, as shown in figure 26. For $\varepsilon << 1$, $\ddot{z}_{Max} \approx gd^4\theta_0^2/l^2k_y^2$ and so

increases very rapidly with the spacing *d*. For ε>1, the maximum angle of yaw is θ_0 = Asinε^{-1}, and for this yaw angle the maximum vertical acceleration is $\ddot{z}_{Max} = 2g/\kappa^2$, and so can become very large for bodies with small yaw gyradii. For example, the present bar on a suspension with *d* = *l* = 1000 mm would have $\ddot{z}_{Max} = 25g$ so the maximum tension in the suspension lines would be some 13 times the weight.

Note: "For ε << 1, $\ddot{z}_{Max} = 2gz_0/l\kappa^2 \approx gd^4\theta_0^2/l^2k_y^2$ for θ_0 << 1, and so increases very rapidly with the spacing *d*." The approximate formula does not work for large angles! Spreadsheet calculation demonstrates the problem with figure 26 Max values calculated from the approximate formula!

Table 4

g =	9.8067	9.8067	9.8067	9.8067
l =	1844	1844	1003	1003
d =	289	289	420	420
k_y =	281	281	281	281
ε^2 =	0.09825	0.09825	0.701385	0.701385
κ^{-2} =	1.05775	1.05775	2.234014	2.234014
θ_0 =	3	1	1.6	0.5
$\ddot{z}_{Max} \approx gd^4\theta_0^2/l^2k_y^2$ =	2.293096	0.254788	9.834347	0.960385
$z_0 = l\left\{1-\sqrt{1-\varepsilon^2 Sin^2(\theta/2)}\right\}$ =	92.45106	20.94016	201.1849	21.76602
$z_0 \approx d^2\theta_0^2/2l$ ~	203.8202	22.64669	225.1167	21.98405
$\ddot{z}_{Max} = 2gz_0/l\kappa^2$ =	1.040128	0.235589	8.788876	0.950861

For a given amplitude θ_0 the vertical acceleration can be calculated as a function of the angular displacement by substitution of $\ddot{\theta}$ and $\dot{\theta}^2$ from equations(0.35) and (0.31) into equation(0.27). Figure 26 shows a comparison of this theory with data for suspensions with ε^2 = 0.098 and κ^{-2} = 1.05 and ε^2 = 0.705 and κ^{-2} = 2.23 at amplitudes of 3.1 and 1.0 radians and 1.6 and 0.5 radians respectively. Equation(0.24) shows that the vertical acceleration is intimately related to the angular acceleration and hence κ, and for small κ can become very large and exert a significant impulsive load on the suspension. The vertical acceleration is not a centripetal acceleration, as is the case for the simple pendulum, as the only rotation is about a vertical axis and the center of mass has purely linear vertical motion.

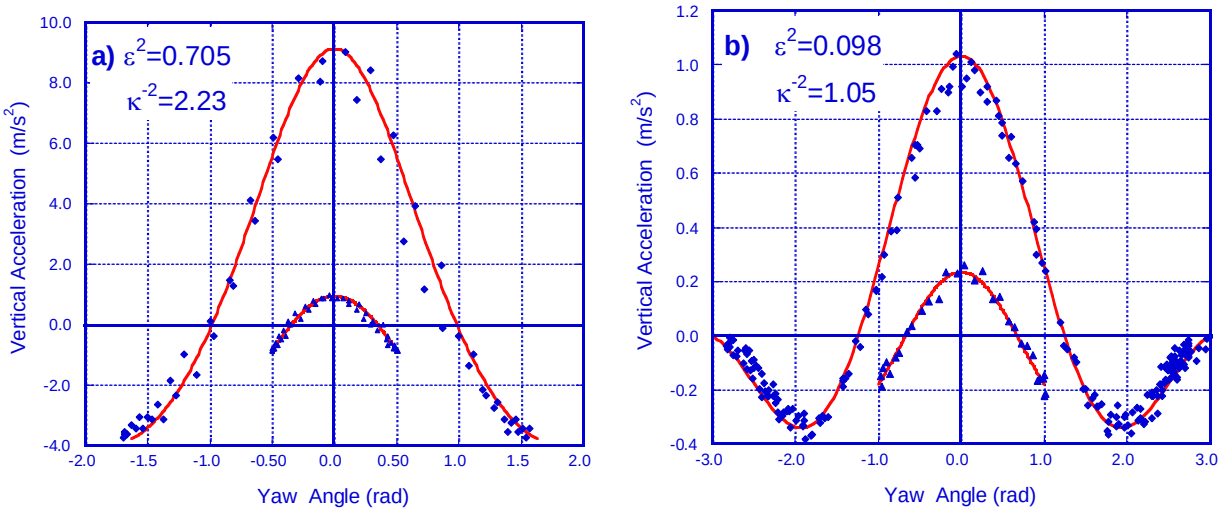

Figure 26 *The vertical acceleration versus yaw angle for a) a suspension with* $\varepsilon^2 = 0.705$ and $\kappa^{-2} = 2.23$ *at* $\theta_0 = 1.6$ *and 0.50 radians and b) a suspension with* $\varepsilon^2 = 0.098$ *and* $\kappa^{-2} = 1.05$ *at* $\theta_0 = 3.0$ *and 1.0 radians. Note the order of magnitude difference in scale. The solid lines are the equation(0.31) predictions.*

J. Yaw line tensions

The tension *T* in the suspension lines required to produce the vertical acceleration $\ddot{z}$ is $T = M\left(\ddot{z}+g\right)/2Cos\phi = M\left(\ddot{z}+g\right)/2\sqrt{1-\varepsilon^2 Sin^2\left(\theta/2\right)}$ and the torque about the vertical axis is $\Gamma = 2Td\ Sin\phi\ Cos\left(\theta/2\right) = 2Td\varepsilon Sin\left(\theta/2\right)Cos\left(\theta/2\right) = Td\varepsilon Sin\theta = Mk_y^2\ddot{\theta}$ so alternatively the line tension is $T = Ml\kappa^2\ddot{\theta}/2Sin\theta$. Thus either of these equations can be used to derive the line tension as a function of yaw angle from the iPhone data. In order to measure the line tensions with the Pasco Force gauges the x, y, and z components would have had to be separately measured and then combined, and this was considered too complex.

Substituting the measured vertical accelerations into equation(0.23) allows the line tensions *T* to be calculated, as shown in figure 27, which confirms the assumption that for $\varepsilon < 1$ and small θ_0 the tensions are $T \approx Mg/2$.

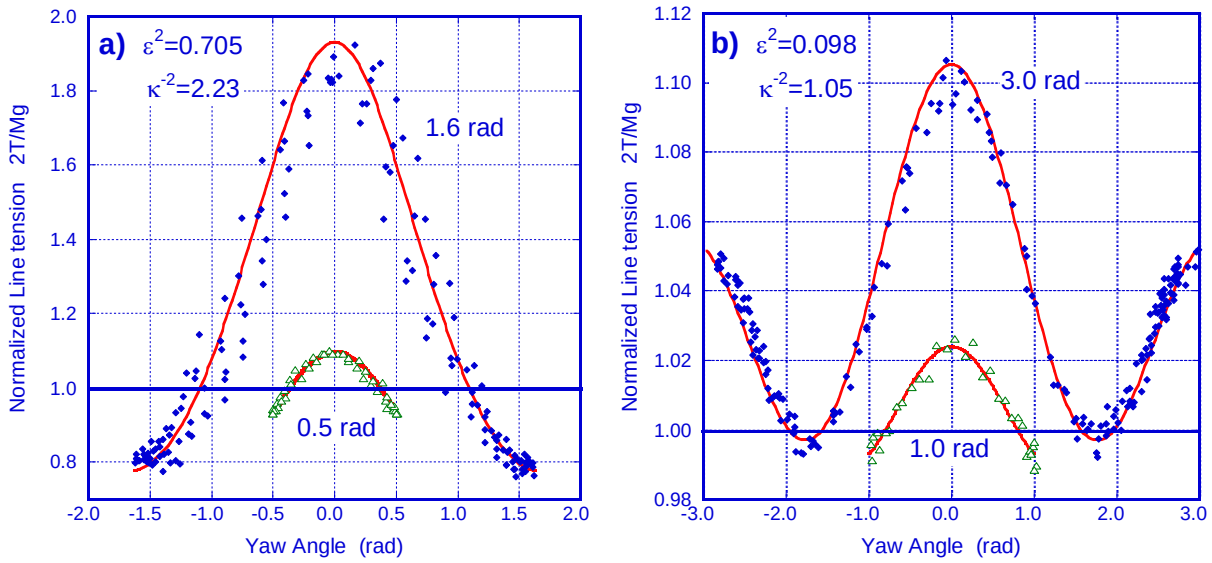

Figure 27 *The normalized line tension versus yaw angle for a) a suspension with* $\varepsilon^2 = 0.705$ and $\kappa^{-2} = 2.23$ *at* $\theta_0 = 1.6$ *and 0.5 radians and b) a suspension with* $\varepsilon^2 = 0.098$ *and* $\kappa^{-2} = 1.05$ *at* $\theta_0 = 3.0$ *and 1.0 radians. The solid lines are the equation(0.23) predictions.*

K. Yaw Angular Velocities and Accelerations

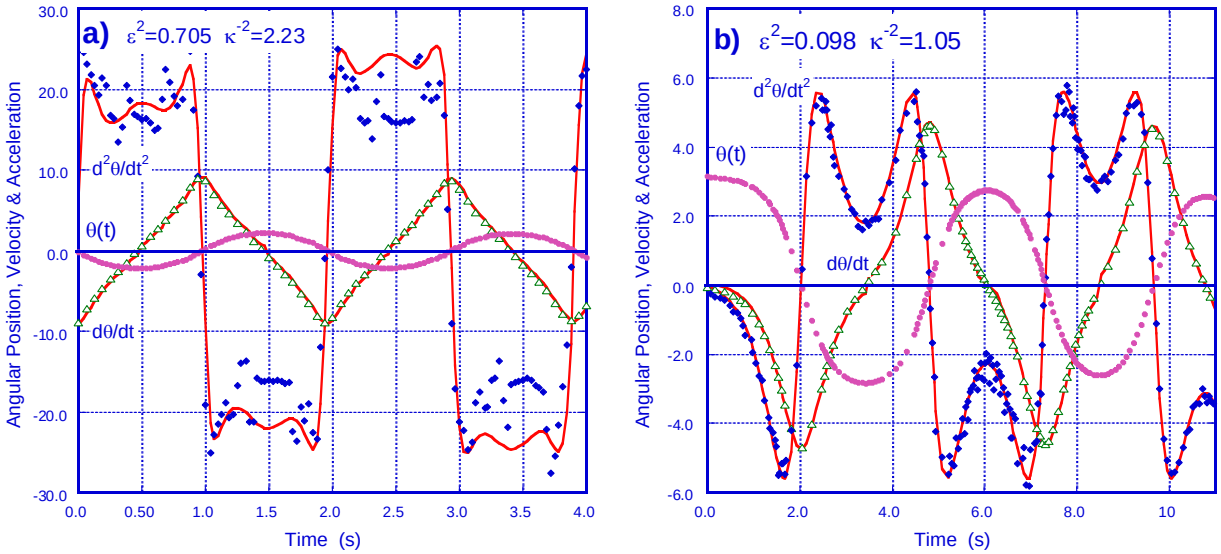

Figure 28 *The angular position (circles), velocity (open triangles) and acceleration (diamonds) versus time for a) a suspension with* $\varepsilon^2 = 0.705$ and $\kappa^{-2} = 2.23$ *at* $\theta_0 = 2.3$ *radians and b) a suspension with* $\varepsilon^2 = 0.098$ *and* $\kappa^{-2} = 1.05$ *at* $\theta_0 = 3.0$ *radians. Note the difference in scales. The solid lines are the predictions of equations(0.31) and(0.35).*

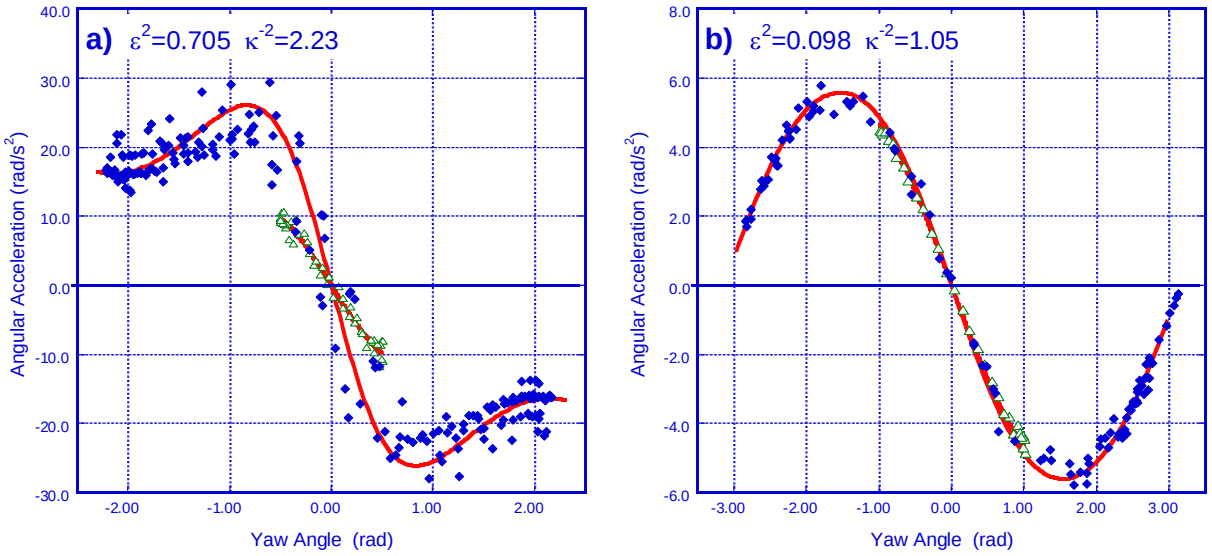

Figure 29 *The angular acceleration versus yaw angle for a) a suspension with* $\varepsilon^2 = 0.705$ and $\kappa^{-2} = 2.23$ *for* $\theta_0 = 2.3$ *(diamond points) and 0.5 (open triangle points) radians and b) a suspension with* $\varepsilon^2 = 0.098$ *and* $\kappa^{-2} = 1.05$ *for* $\theta_0 = 3.0$ *(diamond points) and 1.0 (open triangle points) radians. The solid lines are the predictions of equation(0.35).*

L. Pitch-Surge Double Pendulum Oscillation

Figure 30 *A model sailboat hull in pitch-surge-heave double pendulum oscillation.*

To illustrate the measurement of the CM height *"**a**"* and pitch gyradius k_p, iPhone pitch angle data for a model sailboat hull[17] on a bifilar suspension is presented in figure 31. An initial horizontal displacement perpendicular to the plane of the suspension excited both modes approximately equally and a fit of two sine functions or a FFT[28] then allows the oscillation periods or frequencies to be rapidly extracted. Alternatively, one can resonantly excite only mode 1, and then only mode 2, so such measurements can be made with a simple timer. Subsequently the sway oscillation can be measured and the pitch gyradius and center of mass height extracted from the frequency ratios using equations(0.78) and(0.79). In order to validate the double pendulum method of pitch gyradius measurement and center of mass height measurement a series of data for different suspension lengths were made and are shown in figure 32.

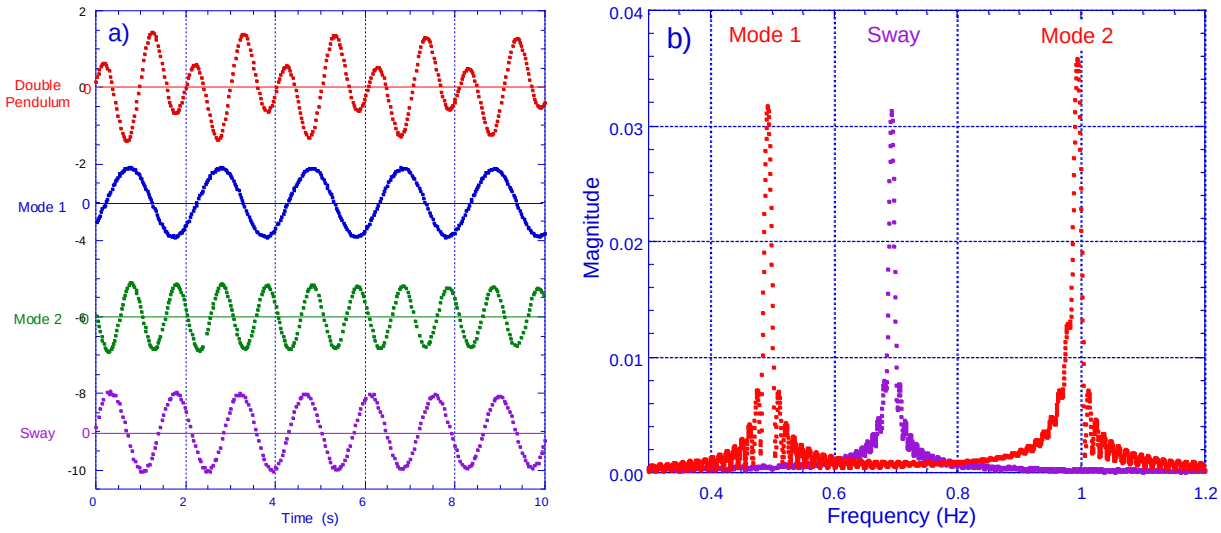

Figure 31 *The pitch-surge-heave double pendulum motion data for a model sailboat hull on a 504 mm bifilar suspension, when displaced horizontally in surge, then separately excited in mode 1, in mode 2 and in sway. The Fourier transforms of the data provide the precise normal mode frequencies.*

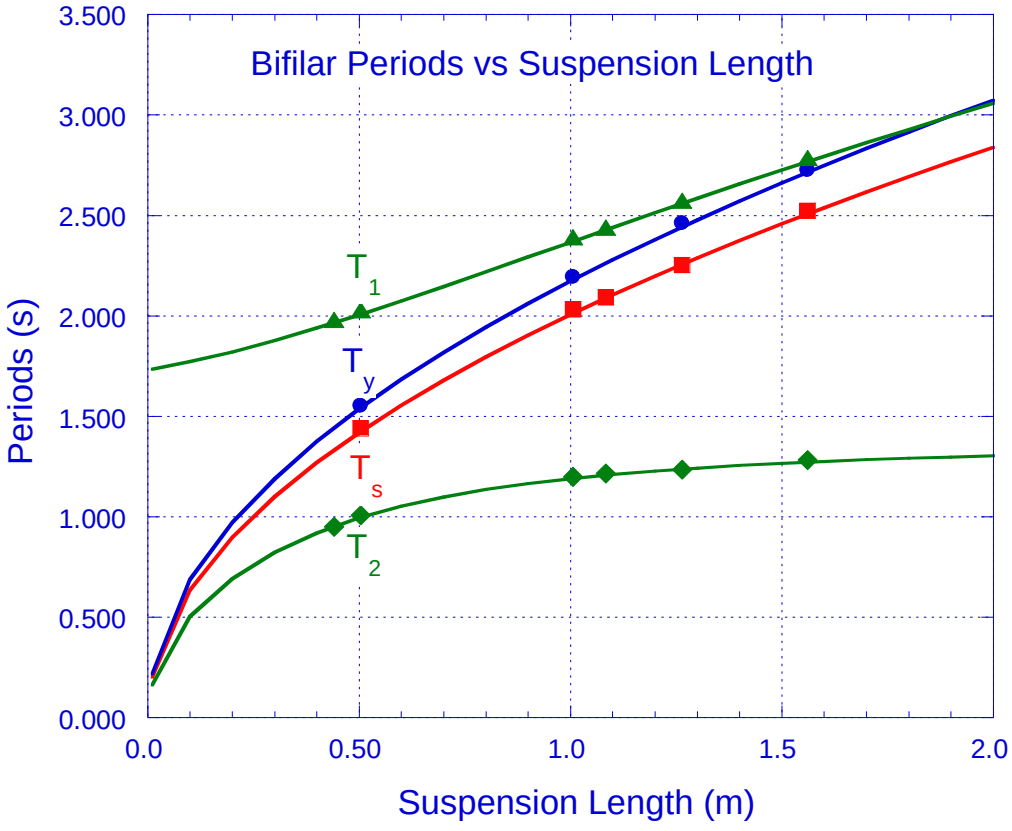

Figure 32 *The model hull oscillation periods T_s of Sway, T_y of Yaw, T_1 and T_2 of double pendulum Modes 1 and 2, as a function of the bifilar suspension length l. The curves are theoretical fits with d = 0.280 m, k_p = 0.352m, k_y = 0.303 m and a = 0.253 m.*

V. Conclusions

A number of the large amplitude oscillatory motions of a body on a bifilar suspension have been investigated using the accelerometers and gyros in an iPhone. The almost universal availability of such MEMs Gyros[31,32] and accelerometers[29] minimizes the cost of the apparatus required while allowing detailed investigation of this and other simple mechanical systems. Isaac Newton was the first to use the bifilar suspension for moment of inertia measurements and it has since been used on full sized aircraft[18] and sailboats[22,17], modern UAVs[19],[20],[21], tank test ship and submarine models[85].

Although the vertical motion associated with the yaw rotation is the essential source of the potential energy, elementary treatments generally ignore the associated kinetic energy. The effects of the vertical motion on the period of yaw oscillation have been investigated as a function of the suspension parameters ε and κ, and a formula for the correction of the yaw period for finite amplitude oscillations has been derived and confirmed.

The precision of such measurements can be significantly enhanced by measuring the ratios of the oscillation periods or frequencies, thus eliminating a number of corrections. Some of the effects of deviations from the ideal symmetrical suspension such as finite mass suspension lines, asymmetrical center of mass have been derived theoretically and investigated experimentally. However, the influence of bearing friction, damping and added mass effects as well as coupling between the modes of oscillation on the measured periods remain to be investigated.

Student laboratories with the bifilar suspension are generally limited to a measurement of the yaw gyradius about a vertical axis and it has been shown that the same suspension can be used to also measure the pitch gyradius about a horizontal axis. Such measurements, which can be applied to a variety of objects of interest to students can even be extended to measurement of all the elements of the inertia tensor by tilting the suspended body. Thus such laboratory experiments can be used to demonstrate the differences in moments of inertia about different axes. The analysis of such data can be limited to the linearized equations or use the full Lagrangian approach, so it can be tailored to the level of the course.

V. Acknowledgements

I would like to thank Jonathan Moscovici for introducing me to “R” and for the numerical integration of equation(0.42).

An abbreviated version of this set of notes has been submitted to the *European Journal of Physics* in April 2015

References

1 Carsten Schedlinski and Michael Link, "A survey of current inertia parameter identification methods," Mechanical Systems and Signal Processing **15** (1), 189-211 (2001).

2 Giancarlo Genta and Cristiana Delprete, "Some considerations on the experimental determination of moments of inertia," Meccanica **29**, 125-141 (1994).

3 Carlo Luigi Bottasso, Domenico Leonello, Andrea Maffezzoli, and Fabio Riccardi, "A procedure for the identification of the inertial properties of small-size UAVs", in *XX AIDAA National Conference* (Milano, Italy, 2009).

4 R Douglas Gregory, *Classical Mechanics*. (Cambridge University Press, Cambridge, 2006), First ed.

5 Herbert Goldstein, *Classical Mechanics*. (Addison-Wesley Publishing Company, New York, 1980), Second ed.

6 Dare A. Wells, *Lagrangian Dynamics*. (McGraw-Hill, New York, 1967).

7 Ross Garrett, *The Symmetry of Sailing: the physics of sailing for Yachtsmen*. (Sheridan House Inc., new York, 1996).

8 Gilbert Lamboley, "Weight Distribution", in *Yachts and Yachting* (1971), pp. 790-793 and 921-924.

9 Gregory L. Baker and James A. Blackburn, *The Pendulum a case study in physics*. (Oxford University Press, Oxford, 2005).

10 M Z Rafat, M S Wheatland, and T R Bedding, "Dynamics of the double pendulum with distributed mass," Am. J. Phys. **77** (3), 216 (2009).

11 Zhi-chao Hou, Yining Lv, and Yao-xin Lao, "A new trifilar pendulum approach to identify all inertia parameters of a rigid body or assembly," Mechanism and Machine Theory (2009).

12 Matt R. Jardin and Eric R. Mueller, "Optimized Measurements of Unmanned-Air-Vehicle Mass Moment of Inertia with a Bifilar Pendulum," Journal of Aircraft **46** (3 May-June) (2009).

13 Paul E Klopsteg, "The bifilar Pendulum," Rev. Sci. Instr. **1** (1), 3-8 (1930).

14 Alan Cromer, "Many Oscillations of a rigid rod," Am. J. Phys. **63** (2 February), 112-121 (1995).

15 F. H. Newman and V. H. Searle, *The General Properties of Matter*. (Edward Arnold & Co., London, 1951), Fourth ed.

16 T. R. Kane and Gan-Tai Tseng, "Dynamics of the Bifilar Pendulum," Int. J. Mech.Sci. **9**, 83-96 (1967).

17 Peter F Hinrichsen, "Bifilar Suspension Measurement of Boat Inertia Parameters," Journal of Sailboat Technology (January), 1-36 (2014).

18 M. W. Green, "Measurement of the Moments of Inertia of full scale Aircraft", in *Technical Notes National Advisory Committee for Aeronautics* (Langley Memorial Aeronautical Laboratory, Washington, 1927), pp. 1-18.

19 Matt R. Jardin and Eric R. Mueller, "Optimized measurements of UAV Mass Moment of Inertia with a Bifilar Pendulum", in *AIAA Guidance, Navigation and Control Conference* (American Institute of Aeronautics and Astronautics, 2007), pp. 23.

20 Matt R. Jardin, "Improving Mass Moment of Inertia Measurements", in *MATLAB Digest* (Mathworks, Maine, 2010), pp. 1-8.
21 Flavio Luiz de Silva Bussamra, Carlos Miguel Montestruque Vilchez, and Julio Cesar Santos, "Experimental Determination of Unmanned Aircraft Inertial Properties", in *3rd CTA-DLR Workshop on Data Analysis and Flight Control*
2009 Brazilian Symposium on Aerospace Eng. & Applications (S. J. Campos, SP, Brazil, 2009).
22 Peter F. Hinrichsen, "Gyradius measurement of Olympic class Dinghies and Keelboats", in *The Tenth Cheasapeake Sailing Yacht Symposium* (SNAME, The Chesapeake Bay Yacht Racing Association, Annapolis, Maryland, USA, 1991), Vol. 10, pp. 1-16.
23 D. Pal and H. A. Gaberson, "Surmounting the Inherent Errors in the Trifilar Pendulum Measurement of Moment of Inertia", in *J. Acoust. Soc. Am.* , edited by SEYMOUR EDELMAN (Acoustical Society of America Statler Hilton Hotel, Boston, Massachusetts 1973), Vol. 54, pp. 292-292.
24 J L du Bois, Naj Lieven, and Sondipon Adhikari, "Error Analysis in Trifilar Inertia Measurements," Experimental Mechanics **49**, 533-540 (2009).
25 Aaron J Swank, Doctoral, http://gradworks.umi.com/3364514.pdf Stanford University, 2009.
26 Aaron J Swank, "Precision Mass Property Measurements using a Five-wire Torsion Pendulum", (NASA Glenn Research Center. Cleveland, www.aspe.net/publications/Short%20Abstracts%2012A/3599.pdf, 2012).
27 Gilbert Lamboley, International Finn Association Technical Committee Report, 1971.
28 George Lungu, A Fourier Transform Model in Excel (www.excelunusual.com, 2012).
29 Gulf Coast, USB Accelerometer Model X6-2 (www.gcdataconcepts.com, 2010).
30 xSensor, "iPhone App," Crossbow Technologies Inc. (2010).
31 MicroStrain, Micro Strain 3DM-GX1 Gyro Enhanced Orientation Sensor (2010).
32 NODE +, Variable Inc., 100 Cherokee Blvd. Suite 327 Chattanooga TN 37405, http://variableinc.com/products/ (2014).
33 Robert A. Nelson and M. G. Olsson, "The Pendulum-Rich physics from a simple system," Am. J. Phys. **54** ((2) February), 112-121 (1986).
34 S. C. Zilio, "Measurement and analysis of large-angle pendulum motion," Am. J. Phys. **50** (5, May), 450-452 (1982).
35 Jerry B. Marion, *Classical Dynamics*. (Academic Press, New York, 1970), Second ed.
36 C.Schwarz, "The not so Simple Pendulum," The Physics Teacher **33** (1995).
37 David P. Jackson, "Rendering the "Not-So-Simple" Pendulum Experimentally Accessible," The Physics Teacher **34** (February), 86-90 (1996).
38 James O'Connell, "Tension in a Pendulum String," The Physics Teacher **40** (January), 24-26 (2002).
39 Ben Szapiro, "Simple-Pendulum Lab with a Twist," The Physics Teacher **40** (March), 158-164 (2002).
40 Julio V. Santos-Benito and Albert Gras-Marti2, "Ubiquitous drawing errors in the Simple Pendulum," The Physics Teacher **43**, 466-468 (2005).

41 Martin Lieberherr, "Figuring the Acceleration of the Simple Pendulum," The Physics Teacher **49**, 576- (2011).
42 Wikipedia, "Elliptic Integral", (http://en.wikipedia.org/wiki/Elliptic_integral,, 2012).
43 Terry R. McConnel, "The Pendulum Period Expansion via Canonical Perturbation Theory", in *TR MCCONNELL http// barnyard.syr.edu/pendulum.pdf* (SYRACUSE UNIVERSITY, barnyard.syr.edu/pendulum.pdf), pp. 15.
44 F. S. M. Lima and P. Arun, "An accurate formula for the period of a simple pendulum oscillating beyond the small angle regime," Am. J. Phys. **74** (10), 892-895 (2006).
45 Kim Johannessen, "An anharmonic solution to the equation of motion for the simple pendulum," European Journal of Physics **32** (2) (2011).
46 Semjon Adlaj, "An Eloquent formula for the perimiter of an ellipse," Notices of the AMS **59** (8), 1094-1099 (2012).
47 Claudio G. Carvalhaes and Patrick Suppes, "Approximations for the period of the simple pendulum based on the arithmetic-geometric mean," Am. J. Phys **76** (12), 1150-1154 (2008).
48 C. G. Montgomery, "Pendulum on a massive cord," Am. J. Phys. **46** (4, April), 411-412 (1978).
49 S. T. Epstein and M. G. Olsson, "Comment on "Effect of the mass of the cord on the period of a simple pendulum."," Am. J. Phys. **45** (7, July), 671-672 (1977).
50 J S Deschaine and B H Suits, "The hanging cord with a real tip mass," European Journal of Physics **29**, 2011- (2008).
51 R. Simon and R. P. Riesz, "Large amplitude simple pendulum: A Fourier analysis," Am. J. Phys. **47** (10, October), 898-899 (1979).
52 L. P. Fulcher and B. F. Davis, "Theoretical and experimental study of the motion of the simple pendulum," Am. J. Phys. **44** (1, January), 51-55 (1976).
53 Donald E. Hall, "Comments on Fourier analysis of the simple pendulum," Am. J. Phys **49** (8) (1981).
54 A Belendez, E Arribas, M Ortuna, S Gallego, A Marquez, and I Pascual, "Approximate solutions for the nonlinear pendulum equation using a rational harmonic representation," Computers and Mathematics with Applications **64** (6), 1602-1611 (2012).
55 Riccardo Borghi, "Simple pendulum dynamics: revisiting the Fourier-based approach to the solution", (arXiv.org > physics > arXiv:1303.5023v1, 2013).
56 Salvador Gil, Andres E. Legarreta, and Daniel E. Di Gregorio, "Measuring anharmonicity in a large amplitude pendulum," Am. J. Phys. **76** (9), 843-847 (2008).
57 J. R. Acton and P. T. Squire, *Solving Equations with Physical Understanding*. (Adam Hilger Ltd., Bristol, 1985).
58 John Nicholas Newman, *Marine Hydrodynamics*. (The MIT Press, Cambridge, Massachusetts, 1977).
59 Frank S. Malvestuto and Lawrence J. Gale, "Formulas for Additional Mass corrections to the Moment of Inertia of Airplanes," Technical Note National Advisory Committee for Aeronautics (1187), 28 (1947).
60 Huw Williams, "Measuring the Inertia Tensor", in *IMA Mathematics 2007 Conference* (IMA, Manchester, 2007).

61 L R Wilberforce, "On the Vibrations of a Loaded Spiral Spring.," Philosophical Magazine **38 Fifth Series**, 386-392 (1894).

62 Peter Hinrichsen, "Bifilar Suspension Measurement of Boat Inertia Parameters," Journal of Sailboat Technology, **To be published**, 34 (2014).

63 John W Conklin, Aaron Swank, Ke-Xun Sun, and Dan B DeBra, "Mass Properties Measurement for Drag-free Test Masses," Journal of Physics: Conference Series **154** (1), 1-7 (2009).

64 "Improved Measurement Method for the Identification of the Centre of Gravity Location and of the Inertia Tensor of Rigid Bodies."

65 A L Korr and Paul Hyer, "A trifilar Pendulum for the determination of Moments of Inertia", (Frankford Arsenal, Research and Development Group, Pitman-Dunn Laboratories, www.dtic.mil/dtic/tr/fulltext/u2/287534.pdf Frankford Arsenal, Philadelphia 37, PA, 1962).

66 Jan Awrejcewicz, *Classical Mechanics: Dynamics*. (Springer, New York, 2012).

67 F. Auerbach and W. Host, *Handbuch der Physikalischen und Techinschen Mechanik*. (Verlag von Johann Ambrosius Barth, Leipzig, 1930), Zweiter Teil ed.

68 W. Veltmann, "Ueber ie Bewebung einer Glocke," Dinglers polytechnisches Journal **22**, 481-494 (1876).

69 G. Hamel, *Element Mechanik*. (Leipzig, 1912).

70 Jeremy S. Heyl, "The Double Pendulum Fractal", (www.tphys.physik.uni-tuebingen.de/...3.../20080811183757!Double.pdf, 2008).

71 Frank Varosi and James A. Yorke, "Chaos and Fractals in Simple Physical Systems ", (University of Maryland, I.P.S.T. College Park, Md 20742, USA, 1991).

72 A Ohlhoff and P H Richter, "Forces in the double pendulum," Z. angew Math. Mech. **00**, 1-22 (2006).

73 Carl W Akerlof, "The Chaotic Motion of a Double Pendulum," http://instructor.physics.lsa.umich.edu/adv-labs/Chaotic%20Double%20Pendulum/Pendulum_2010_04_12.pdf, 24 (2010).

74 Murray R. Spiegel, *Theoretical Mechanics*. (McGraw-Hill, New York, 1967).

75 Wikipedia, "Double pendulum", (http://en.wikipedia.org/wiki/Double_pendulum, 2011).

76 R. C. de Jong and J. A. Mulder, "Accurate Estimate of Aircraft Inertia Characteristics from a Single Suspension Experiment," J. Aircraft **24** (6), 362-370 (1987).

77 R C de Jong, MSc, Delft University ofTechnology, 1985.

78 Pasco, DataStudio (Pasco Scientific, San Francisco, 2000).

79 Peter F Hinrichsen, "Pendulum Bearing Friction", in *In preparation* (www.researchgate.net/profile/Peter_Hinrichsen3/publications, 2014).

80 SPSSScience, TableCurve 2D (http://www.sigmaplot.com/products/tablecurve2d/tablecurve2d.php, Systat Software Inc., San Jose, CA, 2000).

81 Buticov, "Free Oscillations and Rotations of a Rigid Pendulum: Summary of the Theory", (butikov.faculty.ifmo.ru/Pendulum/Manual3.pdf), pp. 21.

82 Karlheinz Ochs, "A comprehensive analytical solution of the nonlinear pendulum " European Journal of Physics **32** (2), 479-490 (2011).

83 Masatsugu Suzuki and Itsuko S. Suzuki, 2008.

84 Wen Hou, "Measuring Moment of Inertia Based on Identification of Nonlinear System Featuring Naught Excitation", in *5th WSEAS Int. Conf. on Instrumentation, Measurement, Circuits and Systems* (Hangzhou, China, 2006).
85 Taran Card, "Bifilar Swinging Experiment," National Research Council Canada, Institute for Marine Dynamics (LM-2000-01), 1-28 (2000).